DEVELOPMENT AND MODELING OF A DUAL-FREQUENCY MICROWAVE
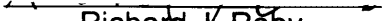# BURN RATE MEASUREMENT SYSTEM FOR SOLID ROCKET PROPELLANT
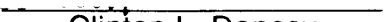
by

DAVID T. FOSS

Thesis submitted to the Graduate Faculty of Virginia Polytechnic Institute and
State University in partial fulfillment of the requirements for the degree of

MASTER OF SCIENCE
in
Mechanical Engineering

APPROVED:

Richard J. Roby

Walter F. O'Brien, Jr.   Clinton L. Dancey

June 1989
Blacksburg, Virginia

DEVELOPMENT AND MODELING OF A DUAL-FREQUENCY MICROWAVE BURN RATE MEASUREMENT SYSTEM FOR SOLID ROCKET PROPELLANT

by

David T. Foss
Committee Chairman: Richard J. Roby
Mechanical Engineering

(ABSTRACT)

A dual-frequency microwave burn rate measurement system for solid rocket motors has been developed and is described. The system operates in the X-band (8.2-12.4 Ghz) and uses two independent frequencies operating simultaneously to measure the instantaneous burn rate in a solid rocket motor. Modeling of the two frequency system was performed to determine its effectiveness in limiting errors caused by secondary reflections and errors in the estimates of certain material properties, particularly the microwave wavelength in the propellant. Computer simulations based upon the modeling were performed and are presented. Limited laboratory testing of the system was also conducted to determine its ability perform as modeled.

Simulations showed that the frequency ratio and the initial motor geometry (propellant thickness and combustion chamber diameter) determined the effectiveness of the system in reducing secondary reflections. Results presented show that higher frequency ratios provided better error reduction. Overall, the simulations showed that a dual frequency system can provide up to a 75% reduction in burn rate error over that returned by a single frequency sytem. The hardware and software for dual frequency measurements was developed and tested, however, further instrumentation work is required to increase the rate at which data is acquired using the methods presented here. The system presents some advantages over the single frequency method but further work needs to be done to realize its full potential.

ACKNOWLEDGEMENTS

In the dark and unfriendly world of research, where the path is sometimes unseen and dangers (or just dissapointments) seem to lurk in every shadow, Dr. Richard J. Roby was always there to lead the way and throw light on the problem with his eternal optimism, insightful intellect and confidence. Rick is one of those all around good-guys (even though he's a Democrat) who always provided good conversation and advice. I'm proud to have been his first grad student, and hope I can live up to that honor.

TABLE OF CONTENTS

LIST OF FIGURES

LIST OF TABLES

NOMENCLATURE

A	Peak-to-Peak voltage of microwave signal on oscilloscope
δ	Distance of propellant burn during time dt
$d\phi_b$	Phase change of burn rate vector over time dt
$d\phi_c$	Phase change of total vector over time dt
$d\phi_1$	Differential phase change of burn rate vector for frequency 1
$d\phi_2$	Differential phase change of burn rate vector for frequency 2
$\Delta\phi$	Phase change
$\Delta\phi_b$	Phase change of the burning surface vector for a change in propellant thickness of δ
$\Delta\phi_s$	Phase change of the secondary vector for a change in propellant thickness of δ
Δx	Change in position of reflector
F1	Frequency 1
F2	Frequency 2
f_1	Frequency of signal 1
f_2	Frequency of signal 2
κ	Burn rate constant equal to $1/4\pi$
λ	Microwave wavelength
λ_c	Microwave wavelength in the combustion chamber
λ_p	Microwave wavelength in the propellant
L	Combustion chamber diameter
L_p	Propellant thickness
n	Order of secondary reflection
$\dot{\phi}(t)$	Time rate of phase change

$\dot{\phi}_{b1}(t)$ Time rate of phase change for burning surface vector, frequency 1

$\dot{\phi}_{b2}(t)$ Time rate of phase change for burning surface vector, frequency 2

$\dot{\phi}_{sn}(t)$ Time rate of phase change for the n-th order secondary reflection

ϕ_{s1} Initial phase of secondary reflection vector

ϕ_{s2} Final phase of secondary reflection vector

r   Propellant burn rate

1. INTRODUCTION

1.1 Background and Literature Review

Measurement of the burn-rate in a solid propellant rocket motor is critical to the testing of existing designs and the development of new, higher performance rocket motors. Pressure-derived burn rate data is only accurate at the point of measurement (usually the head end of the combustion chamber). If chamber pressures vary along the combustion chamber length, the measurement will not be valid in other areas of rocket motor.

Development of advanced solid propulsion systems such as nozzleless and pulsed rocket motors creates an increasing need for accurate, non-intrusive burn rate measurement systems. Such propulsion systems feature either time or spatial variations in burn rates or a combination of both. Active control of combustion in rocket motors is another area where real-time, non-intrusive sensors are needed to measure burn rates. Clearly the pressure measurement methods are inadequate for these applications.

Various other burn rate measurement techniques such as X-ray video and ultrasonics have numerous advantages over pressure measurements, such as high spatial resolution and non-intrusive measurement. The disadvantages of these techniques include the high cost and complexity of the X-ray video and environmental sensitivity (vibration of the rocket motor during operation) of the ultrasonic technique. The use of microwaves to provide non-intrusive measurement of solid propellant burn rates overcomes some of the disadvantages of the above techniques, though data acquisition and reduction is a major problem.

The burn rate (or regression rate) of the propellant is measured by passing microwave radiation through a rocket motor casing and propellant and capturing the radiation reflected off the moving burning surface. The phase of this reflected radiation is

1

compared with that of the incident (or reference) signal. The phase change between the two signals contains information related to the change in thickness of the propellant. Continuous calculation of this phase change over time yields the data necessary for burn rate calculations.

The ability to measure the phase change of the signal reflected off the propellant/combustion chamber interface, to the exclusion of other reflections, is critical. The correlation between the burn-rate and the phase change is given in the following equation

$$r = \dot{\phi}(t)\lambda/4\pi \qquad\qquad [1.0]$$

where $\dot{\phi}(t)$ is the time rate of phase change of the burning surface reflection.

λ is the wavelength of microwave radiation.

4π converts phase change into wavelengths (2π) and halves the result since reflections travel through the propellant twice.

A microwave measurement system based upon these principles was developed at VPI&SU and discussed in a thesis by Holly [1]. This system was designed for use with a slab rocket motor to provide a neutral burning environment where pressure derived data was fairly accurate. Holly also developed a two-vector model of the microwave reflections. This provided the basis for a data reduction scheme used with the system. Holly conducted tests of the system using a device which moved a metal plate in front of the microwave horn to provide a moving reflection surface.

Test results for the microwave system and slab motor combination were first presented by Wood, O'Brien, and Dale [2]. This paper also describes the data reduction technique based on Holly's two-vector model. A more in-depth examination and description of the slab motor testing is contained in a thesis by Kliger [3]. Kliger presented results of the use of the data reduction technique applied to both computer simulated microwave data, and the actual slab motor firings. Comparisons between the

six slab motor firings, computer simulated firings, and the burn rate data from pressure measurements were also made by Kliger. The testing showed the microwave measurements agreed with pressure-derived measurements to within ten percent. Multiple reflections of the microwave signal off various surfaces within the rocket motor tended to reduce the accuracy of the system.

Boley [4], in his thesis, developed a more complex model of the microwave reflections. This resulted in a data reduction technique which calculated reflections based upon the material properties of the rocket motor and propellant. This new technique was applied to both simulated data and data from the earlier slab motor testing. Boley showed that small errors (+/- 1%) in material properties (particularly the propellant) resulted in much larger errors in calculated burn rates.

In 1987, Waesche and O'Brien [5] examined the three non-intrusive measurement techniques discussed earlier. All provide an equivalent level of spatial resolution but accuracy and ease of use are dissimilar. The authors concluded that measurement errors of less than 1% are necessary for a system to examine relevant phenomena in the rocket motor environment. The microwave technique was found to have a theoretical measurement error of much less than one percent. The major obstacle to achieving such accuracy was found to be the errors in material properties as concluded by Boley. Thus, elimination or suppression of material property errors should be the major focus of further microwave measurement system development.

1.2 Current Approach

This thesis describes an attempt to solve the material property problem by developing a dual-frequency microwave measurement system. The original system described by Holly and Kliger was modified to operate simultaneously with two microwave frequencies. By using two frequencies simultaneously, two sets of data are

acquired which measure the same phenomena. Modelling of the dual frequency reflections results in several relationships which can be used to eliminate the need to estimate material properties and reflection vectors.

The use of two frequencies can also help find accurate values of the microwave wavelength in the propellant. Since the ratio of the frequencies is the inverse of the ratio of the microwave wavelengths within the propellant, values of wavelength can be iterated until both burn rate curves (from each frequency) and the wavelength/frequency ratios match. These conclusions are based upon the assumption that the signal at each frequency is independent in the rocket motor, and each can be measured independently. Another key assumption is that the wavelength of the microwaves in the propellant changes linearly with the changes in frequency. In the present research this was assumed to be true for the small bandwidth being considered (8.5 to 11.5 Ghz). Over a larger bandwidth variations in the material dielectric constant becomes non-linear with linear frequency changes.

This thesis describes in detail the two-frequency modeling which was done to support the basic assumptions and to show the veracity of the two-frequency technique. Various computer simulations of two frequency microwave measurements are presented which show the effects of using the technique under various conditions. Some simulations were modifications of earlier work done by Kliger, while others represent different rocket motor geometries. Frequencies used were also varied to determine the effect of such measurements on the resulting data.

The new two-frequency microwave system, and the new diagnostic and measurement instrumentation used with it are described in detail. Although designed with full scale testing in mind, due to limitations in the instrumentation, testing was limited to simply verifying its intended function. Data acquisition and reduction of data from a full

scale test is described but not fully implemented. Descriptions of the test apparatus and testing technique for conducting a laboratory test are also included.

Finally, recommendations are made for overcoming the instrumentation problems encountered and improving the system in preparation for actual live rocket motor testing. These include improvements to the hardware such as the microwave sources and test equipment. Suggestions are also made for improving the data reduction techniques.

2.   MODELING OF TWO FREQUENCY SYSTEM

Microwave radiation which is incident upon a dielectric material such as a composite rocket motor casing or the rocket propellant has is partially reflected and partially transmitted depending upon the electromagnetic properties of the material. The wavelength of the microwaves in a material will also vary from the free space value depending upon the material's particular properties. Reflections will therefore occur at each interface in the rocket motor where the material changes. As seen in figure 1 (from reference [5]), a typical rocket motor has several material interfaces which will cause reflections of different intensity if microwaves are directed through the motor perpendicular to the motor's axis. The reflection's intensity is again a function of the materials in question.

The basis for mathematically modeling these reflections is to represent them as two-dimensional vectors, or more properly phasors, whose magnitude and phase represent the magnitude and phase of the reflected microwaves. In this thesis, magnitudes are in millivolts and phase is in radians. Phasors can be created which represent the individual reflections from each interface. These individual phasors can then be added to give a single total phasor which represents the reflection measured by the microwave instrumentation. The following sections describe the modeling done for operation using a single frequency which is then expanded into the use of two frequencies simultaneously.

2.1   Model Development

Previous research efforts dealing with microwave measurement systems were deeply involved in developing models of the various reflections from different material interfaces. These models enabled estimation of the magnitude and phase of the different
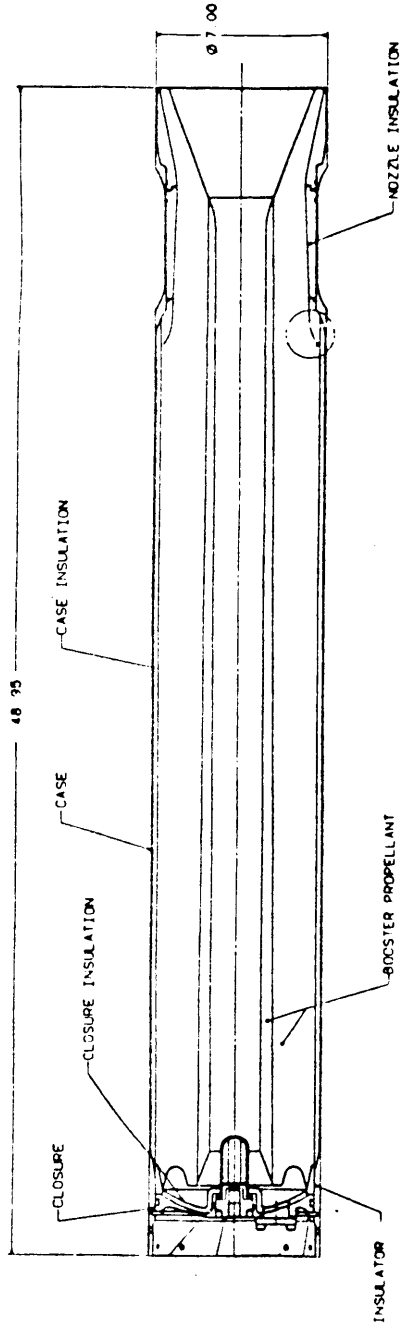
Figure 1. Cross section of a nozzleless rocket motor (from reference [5]).

reflection vectors so that the data on the reflection vector from the burning surface could be retrevied from the raw data. Unfortunately, these models relied heavily on knowledge of the local material properties which were hard to measure accurately and could change due to environmental influences (heat and pressure in the rocket motor). In addition, the models are only valid for an individual rocket motor and would have to be greatly modified for each type of motor tested. (Changes in materials and material thickness from one motor type to another require changes in the model).

Elimination of the requirement to estimate individual reflection vectors would greatly improve the practicality and accuracy of the microwave measurement system. The rational behind the simultaneous use of two frequencies is that unwanted reflections associated with each frequency can be eliminated due to their ratios being related to the ratio of the frequencies used. There is also the fact that the measurement of burn rate from one frequency signal must equal the measurement from the second frequency signal.

Looking first at the cross section of a generic rocket motor in figure 2, there are two material layers beginning with the structural casing/insulating layer, then the propellant. At each material interface, incident microwave energy is both reflected and transmitted. The reflection of interest is, of course, the reflection from the propellant burning surface. Unfortunately, all reflected radiation is combined into a single signal which is picked up by the measurement equipment.

Development of the present model begins with a vector representation of microwave reflections in figure 3. This figure shows the total vector $V_c(t)$ which is theresultant of combining the vectors representing reflections from fixed surfaces (V_{f1}, V_{f2}) and the reflection from the propellant/combustion chamber interface, $V_b(t)$. The total vector, $V_c(t)$, can easily be measured in both magnitude and phase relative to the input radiation. Figure 4 combines the fixed vectors into a single vector $V_a(t)$, which is initially
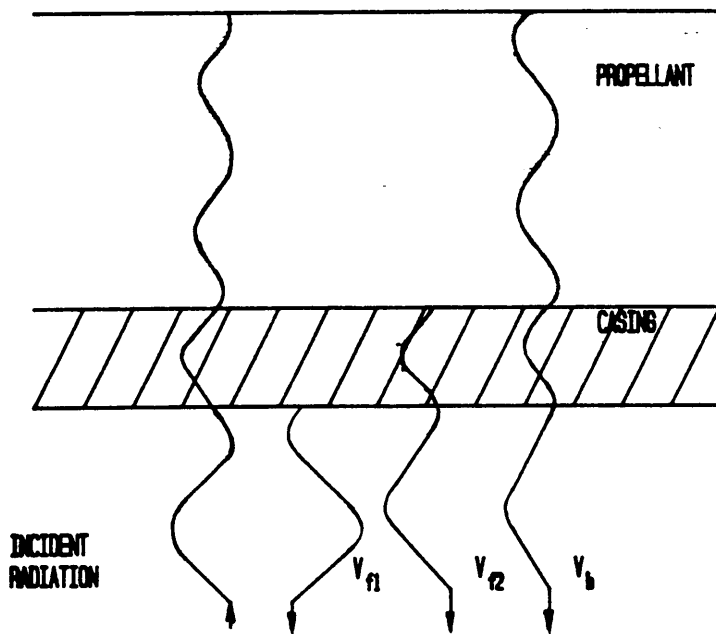
Figure 2. Rocket motor cross section with incident microwave radiation.
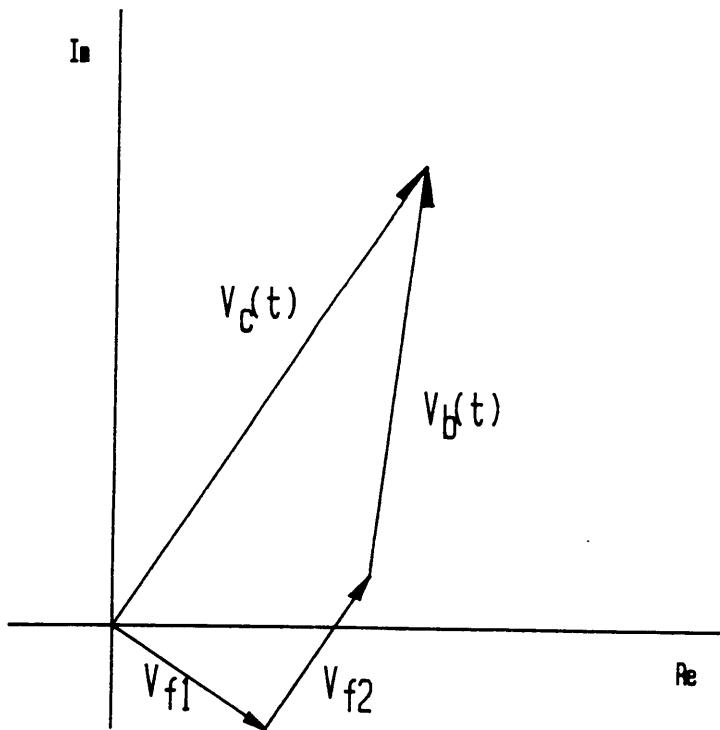
Figure 3. Vector representation of microwave reflections.
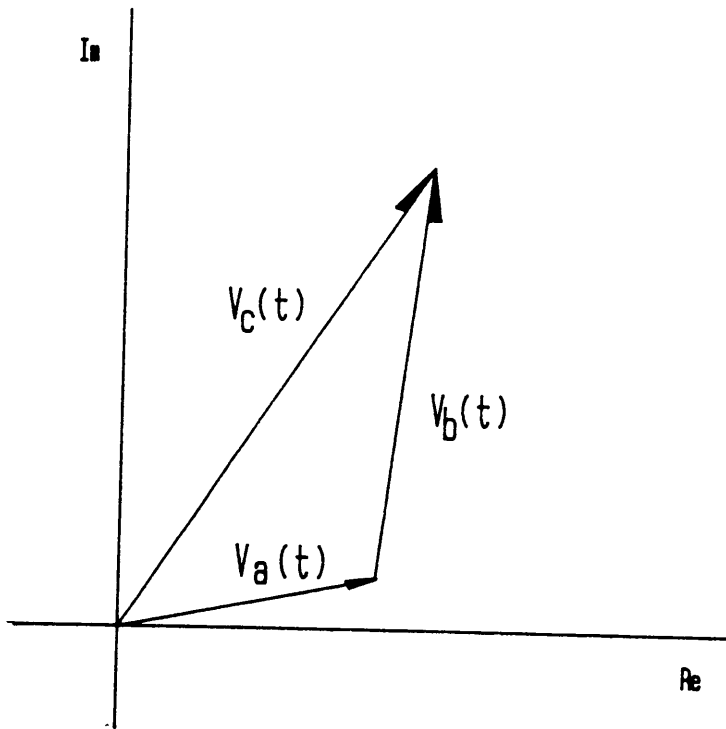
Figure 4. Three vector system with single fixed interface reflection vector.

written as being time dependent. This is true only if the microwave radiation directed at the rocket motor changes in amplitude and phase with time. This results in a three vector system where $V_c(t)$ is known but $V_b(t)$, which contains the relevant phase information, is unknown along with $V_a(t)$.

In previous work described in reference 2, the vector V_a is considered fixed in time since the input radiation is kept fixed in magnitude and phase, and thus the time variance is dropped. A data reduction scheme was developed which allowed calculation of the phase change of $V_b(t)$ knowing only the magnitude and phase of $V_c(t)$. As shown in figure 5, the difference vector of $V_c(t)$, $dV_c(t)$, is calculated from two successive measurements of $V_c(t)$. The rate of phase change of this vector, when calculated for small changes in time, was shown to be equivalent to the rate of phase change of the burning surface vector $V_b(t)$. This results in a simple algorithm which is used to find the rate of phase change of $V_b(t)$ in a two vector system.

We can now look at vector representations for a system with two frequencies operating simultaneously. Figure 6 uses two phase diagrams to show results for each frequency with more clarity. The three vector systems are represented for each of the frequencies, 1 and 2 (frequency 1 is considered the lower frequency while frequency 2 is the higher). Also shown is the change over a time interval of the vectors due to a change in thickness of the propellant. The solid lines represent the state at time t, while the dashed lines represent the state at time t+dt. Over this short time interval $V_c(t)$ has changed phase by $d\phi_c$, while the vector of interest, $V_b(t)$ has changed phase by $d\phi_b$.

Since both frequencies are measuring the same change in thickness of the propellant, dx, the two phase changes of vectors $V_b(t)$ are related as follows.
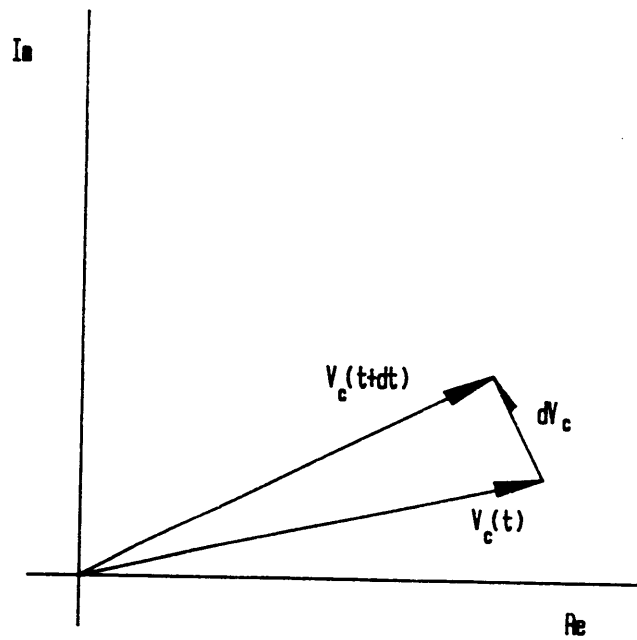
Figure 5. Calculation of difference vector from two successive measurements of the total vector.
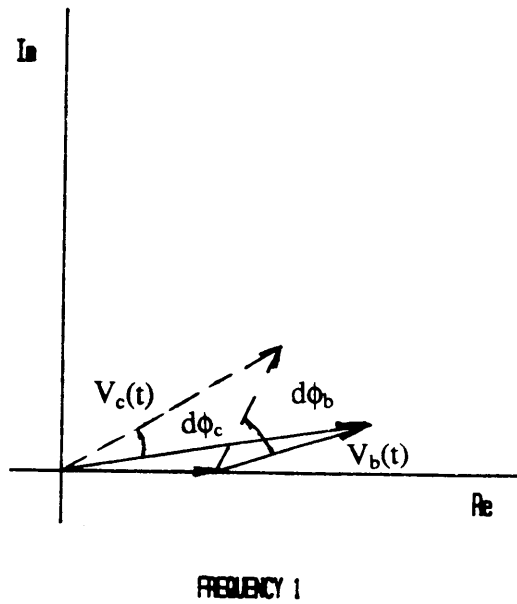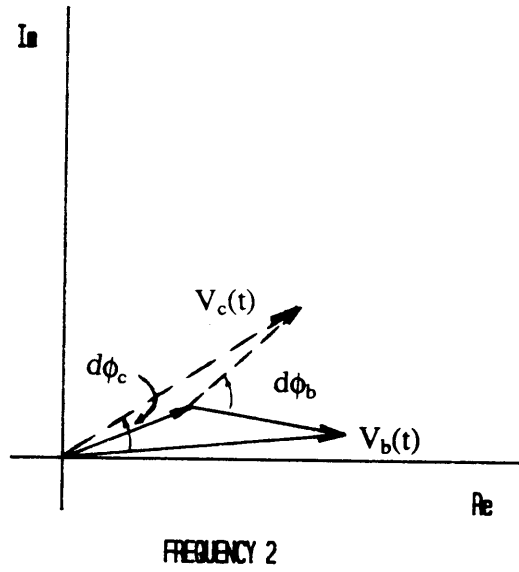
Figure 6. Vector diagrams for two frequencies showing change over a time interval.

$$dx = d\phi_1\lambda_1/4\pi = d\phi_2\lambda_2/4\pi \qquad\qquad [2.1]$$

where $d\phi_1$ and
$d\phi_2$ are the phase angle changes for frequencies 1 and 2.
λ_1 and
λ_2 are the microwave wavelengths in the propellant.

Since the wavelengths are inversely proportional to the frequencies, equation 2.1 can be rewritten as

$$d\phi_1/f_1 = d\phi_2/f_2 \qquad\qquad [2.2]$$

where f_1 represents frequency 1.
f_2 represents frequency 2.

Changing the differential quantities to time derivatives, a system of three equations with three unknowns can be created,

$$r = \kappa\dot{\phi}_{b1}(t)\lambda_1 \qquad\qquad [2.3]$$

$$r = \kappa\dot{\phi}_{b2}(t)\lambda_2 \qquad\qquad [2.4]$$

$$\dot{\phi}_{b1}(t)/\dot{\phi}_{b2}(t) = \lambda_2/\lambda_1 = f_1/f_2 \qquad\qquad [2.5]$$

where κ is $1/4\pi$
$\dot{\phi}_{b1}(t)$ is the time rate of phase change of the burning surface vector, frequency 1.
$\dot{\phi}_{b2}(t)$ is the time rate of phase change of the burning surface vector, frequency 2.

Where the unknowns are λ_1, λ_2 and r.

By iterating through values of the wavelength until the two burn rates match, errors in the measurement of λ and the rate of phase change can be reduced, resulting in a more accurate measure of the burn rate.

These relationships are dependent on the assumption that the fixed interface vectors, represented by V_a are fixed or change slightly as compared with $V_b(t)$, and that the ratio of microwave wavelengths in the propellant is equal to the input frequency ratio within the bandwidth being considered (9.0-11.0 Ghz). Equations 2.3, 2.4, and 2.5 form the basis of the model.

Another method for insuring the accuracy of the values of microwave wavelength is an integration technique. Integration of the burn rate over the total burn time yields the initial web thickness of the propellant, which is easily measured. If a mismatch occurs after integrating the microwave derived data, the value of the microwave wavelength in the propellant can be iterated until a close match occurs. This can be used to correct gross errors in the value of λ, but will not greatly increase the measurement accuracy due to errors in the rate of phase change measurement.

2.2   Modeling of Multiple Moving Vectors

Beyond the errors which occur due to property measurement errors, there are large errors in measurement which occur due to secondary moving vectors in the rocket motor. These vectors usually come in two types. The first, and of lowest magnitude, are reflections which travel through the propellant four, six or eight times before reaching the receiving equipment. These vectors are smaller in magnitude (due to attenuation during the travel through the propellant) but have two, three or four times the rotation rate of the burning surface vector. The second type occurs due to reflections of the microwave signal off the opposite side of the combustion chamber. Depending upon the motor geometry (what is on the opposite side of the combustion chamber to reflect the signal), these vectors usually are larger in magnitude than the first type (less attenuation in the path length) but have a rate of phase change less than that of the burning surface vector. These types of reflections will be examined in detail in this section.

Previous research [3] found that a small magnitude reflection with a large rate of phase change will lead to large errors in burn rate. These vectors greatly affect the burn rate by causing the equivalent of a magnitude oscillation in the burning surface vector which leads to errors in the phase measurement. This type of vector occurs when portions of the microwave radiation reflected off the burning surface fail to penetrate the motor casing, thus returning to the burning surface to be reflected again. At each stage in the reflection from a surface, some radiation will be transmitted. This leads to a reflection vector being returned to the measurement instrumentation which is much smaller in magnitude yet has a phase change rate twice that of the burning surface vector if it travels through the propellant four times (a second order reflection). A third order reflection will be smaller still in magnitude yet have a phase change rate three times that of the burn rate vector after travelling through the propellant six times. The modeling describing these types of vectors was reported by Kliger [3] in his thesis. In these cases, the relationship between rates of phase change can be written as follows.

$$\dot{\phi}_{sn}(t) = n\dot{\phi}_b(t) \qquad\qquad [2.6]$$

where $\dot{\phi}_{sn}(t)$ is the rate of phase change of the n-th order secondary reflection.

n is the order of the reflection.

The second type of reflection which will be prevalent in a rocket motor was also modeled by Kliger, and consists of reflections off the opposite side of the combustion chamber. This modeling dealt only with the slab motor geometry, which had fixed surfaces opposite the propellant slab. For a rocket motor with a cylindrical propellant cross section, the reflection will be affected by the burn rate on both sides of the combustion chamber. Figure 7 shows the axial cross section of a cylindrical rocket motor which has burned a distance of δ during an interval of time. (The burn rates on each side
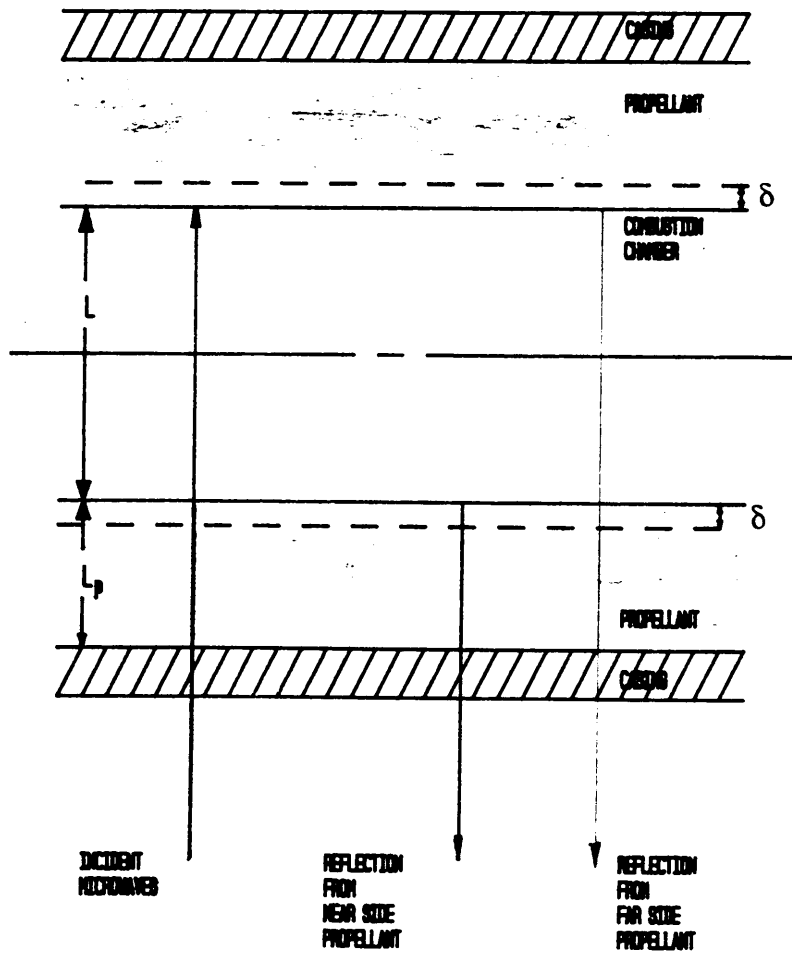
Figure 7. Microwave reflections in a cylindrical rocket motor.

of the combustion chamber at a certain axial location are assumed equal since pressure should be constant through the cross section). The phase change of the burning surface vector is given by the following equation.

$$\Delta\phi_b = 2\delta(2\pi)/\lambda_p \qquad\qquad [2.7]$$

where $\Delta\phi_b$ is the phase angle change of the burning surface vector.

                        λ_p is the microwave wavelength in the propellant.

Calculation of the phase change for the secondary vector is done by calculating phase change due to expansion of the combustion chamber by 2δ and the burning of the propellant by δ. The initial phase before burning is

$$\phi_{s1} = \{2L_p/\lambda_p + 2L/\lambda_c\}2\pi \qquad\qquad [2.8]$$

where ϕ_{s1} is the initial phase angle of the reflection off the opposite burning surface.

                        L_p is the initial propellant web thickness.

                        L is the initial combustion chamber diameter

                        λ_c is the microwave wavelength in the combustion chamber.

while the final phase is

$$\phi_{s2} = \{2(L_p - \delta)/\lambda_p + 2(L + 2\delta)/\lambda_c\}2\pi \qquad\qquad [2.9]$$

where ϕ_{s2} is the final phase angle of the reflection.

Subtracting 2.7 from 2.8 and reducing gives the phase change.

$$\Delta\phi_s = 8\delta\pi/\lambda_p(\lambda_p/\lambda_c - 1/2) \qquad\qquad [2.10]$$

where $\Delta\phi_s$ is the phase change of the far side reflection.

The relationship between $\Delta\phi_b$ and $\Delta\phi_s$ is found by solving for δ in equations 2.6 and 2.9 and equating the results. This leads to the following result.

$$\Delta\phi_s = 2\Delta\phi_b(\lambda_p/\lambda_c - 1/2) \qquad\qquad [2.11]$$

Depending upon the value of λ_p/λ_c the phase change of this vector is likely to be close to zero since the propellant wavelength is close to one half the free space value and estimates of the combustion chamber value are very close to the free space value.

Although this derivation rules out any significant reflection from the far surface of a cylindrical rocket motor, such a reflection can occur in motor geometries where there is no burning surface opposite the measured one. Such situations exist in solid propellant gas generators where propellant is cast in a cylinder and burning occurs on one end only. Kliger did derive the phase change relationship for microwaves travelling through the propellant and reflecting off a fixed surface opposite the burning surface. (This situation existed in the slab rocket motor which was used in the live testing conducted at VPI & SU).

Kliger's derivation showed the relation between the phase change of far surface reflections and the burning surface reflection phase change is represented by the following equation expressed as a time derivative.

$$\dot\phi_{fs} = \dot\phi_b(1 - \lambda_p/\lambda_c) \qquad\qquad [2.12]$$

Since λ_p/λ_c is close to one half, the far side vectors rotate at a rate less than that of the primary burning surface vector.

The two classes of moving reflections which are considered significant are therefore the second and higher order reflections which are small in magnitude but have a much higher rate of phase change than the burning surface vector, and the far side reflection which is relatively large in magnitude with a slower rate of phase change than the burning surface vector. These two types of moving reflections are included in the

simulations to determine the ability of the two frequency system to eliminate or reduce their effects.

The simulations in chapter 3 uses the two frequency modeling presented to develop an understanding of the dynamic behavoir of this type of system. Different types of reflections and different conditions are simulated within the limitations given by the model.

3.   MODEL IMPLEMENTATION

Implementation of the data reduction schemes requires measurement of the phase and magnitude of the total vector $V_c(t)$, the frequencies of the microwaves being used and an initial estimate of one of the microwave wavelengths in the propellant. The total vector magnitude and phase must be sampled at a rate high enough to ensure validity of the calculations which yield the burning surface vector phase change.

Once the burning surface rate of phase change has been calculated (using the difference vector method described in section 2.1) for both frequencies, the burning rate curves can be calculated using equations 2.3 and 2.4. Values for wavelengths would be calculated from the initial estimate and the frequency ratio (equation 2.5).

The two burn rate curves can now be compared to see if they match. A mismatch in the burn rate curves requires iteration of the rate of phase change data until a the burn rate curves match. The wavelength iteration can be done for the total burn using the integration technique or modified to provide a variable wavelength for each phase/magnitude measurement made by the instrumentation. The latter method would allow for propellant inconsistencies and property changes.

In order to check the validity and accuracy of the two frequency model, a computer program was developed which simulates measured microwave data from a set of inputs which are based on some assumptions of microwave behavior in a rocket motor and measurements of the reflectivity of certain materials. A similar single frequency simulation program was used by Kliger and Boley in their work.

3.1   Program Description

The program, MWSIM.FOR (given in Appendix A), takes inputs of magnitude, phase, and rate of phase change for two moving and one fixed vectors. The magnitude and rate of phase change of the two moving vectors can vary linearly to simulate the change in propellant thickness and a varying burn rate. The total vector sum of the three vectors is calculated over the total burning time interval at a specified rate. This total vector data is used to calculate the difference vector and its rate of phase change, from which the burn rate is calculated. A second three vector system is created by the program which is related to the first by an input power ratio, frequency ratio, and initial angle of the vectors.

This results in two sets of data which are related in certain specified ways yet are acting independently. Programs which manipulate the data created by MWSIM.FOR implement the assumptions made in section 2.1. The following subsections describe the simulations, their results and the results of the data reduction programs.

3.2   Computer Simulations

3.2.1 Simulation 1

Simulation 1 is a simple two vector simulation consisting of a fixed vector and the moving burning surface vector. This simulation shows the relationship between the two frequencies and demonstrates the validity of the difference vector reduction algorithm. A second purpose was to demonstrate the use of the integration technique to determine the correct values of the propellant wavelengths.

Table 1 lists the appropriate inputs for this simulation including the power ratio, frequencies and input burn rate, which is input through the rotation rate of $V_b(t)$--the burning surface vector. The magnitudes of vectors are based upon data calculated by Kliger for the simulations he did. This is also true for the propellant wavelength of 1.408 cm which was experimentally determined for the propellant used in the slab motor tests. Initial angles are based upon a web thickness of 3.0 cm and the geometry of the rocket motor. These data are used in most of the other simulations except where indicated.

Figure 8 shows plots of the total vector for frequencies one and two. The initial vector positions are shown, as they are for all simulations. The frequency 2 plot has a smaller magnitude overall, due to the input power ratio, and also goes through a larger absolute phase change, which is due to its higher frequency.

Figure 9 contains plots of the difference vector magnitude and phase for the two frequencies. Both plots are symmetric about the origin and show a different though constant rate of phase change associated with a constant burn rate. The burn rate is calculated by inserting the rate of phase change of these vectors into equation 1.0. In this case a ten percent error in the input wavelength results in a ten percent error in the burn

Table 1. Simulation 1 parameters.

Frequency 1 (Ghz):	9.20		
Frequency 2 (Ghz):	10.45		
Power Ratio (1/2):	1.2		
Vector Magnitudes (mV) for Frequency 1:			
V_a:	10.0		
$V_b(t)$:	20.0 increasing to 24.6		
Vector Rotation Rates (rad/sec) for Frequency 1:			
V_a:	fixed		
$V_b(t)$:	8.925		
Vector Initial Angles (deg):			
V_{a1}:	0.0	V_{a2}:	0.0
$V_{b1}(t)$:	60.0	$V_{b2}(t)$:	160.0
Input Wavelength, Frequency 1 (cm):	1.268		
Propellant Web Thickness (cm):	3.0		
Simulated Burn Rate (cm/sec):	1.0		
Burn Time (sec):	3.0		
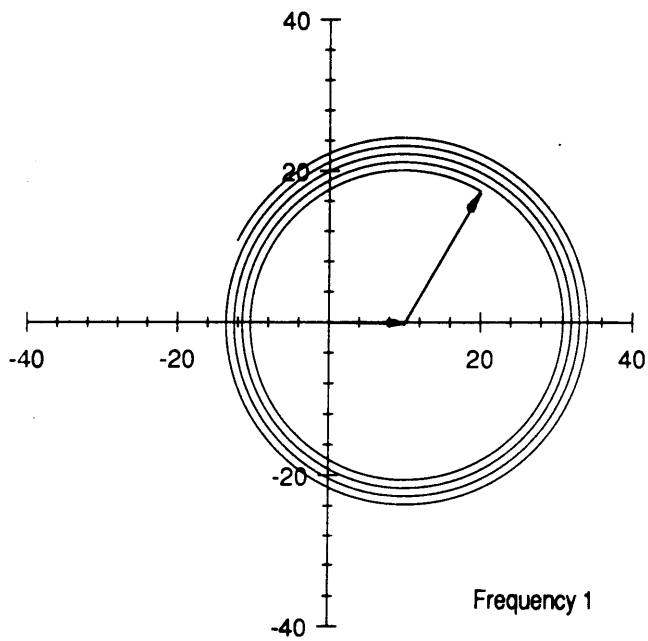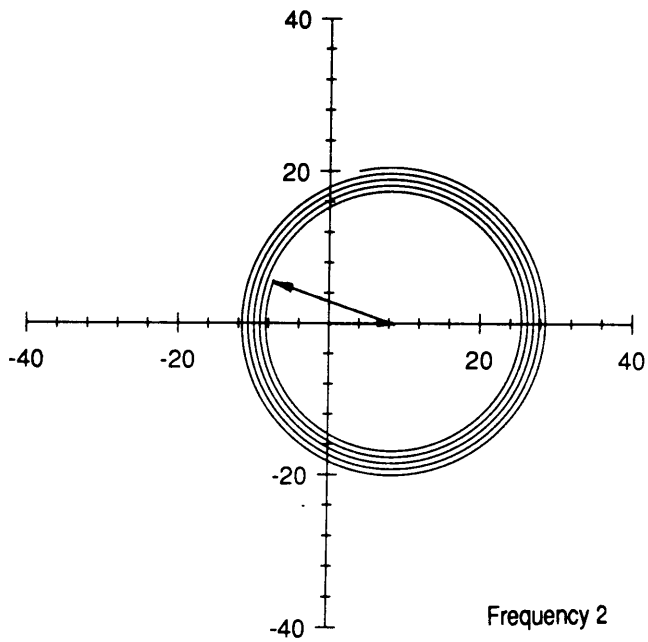
Figure 8. Total vector plots for both frequencies for Simulation 1.
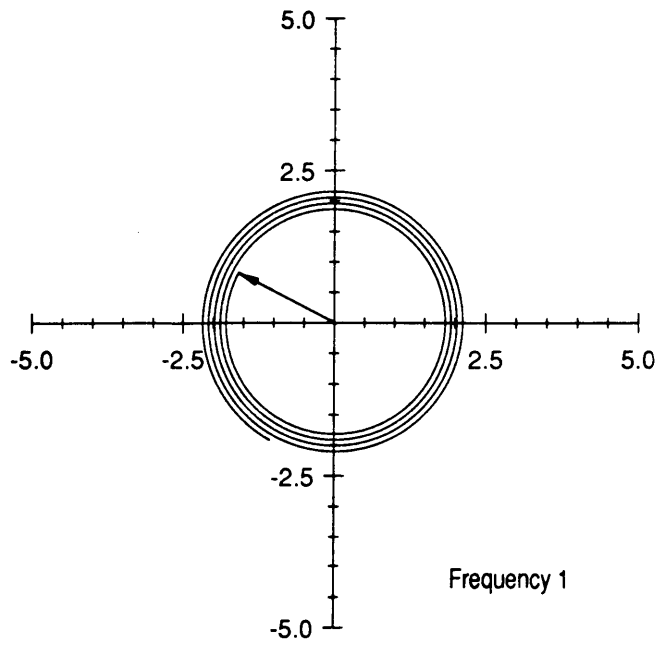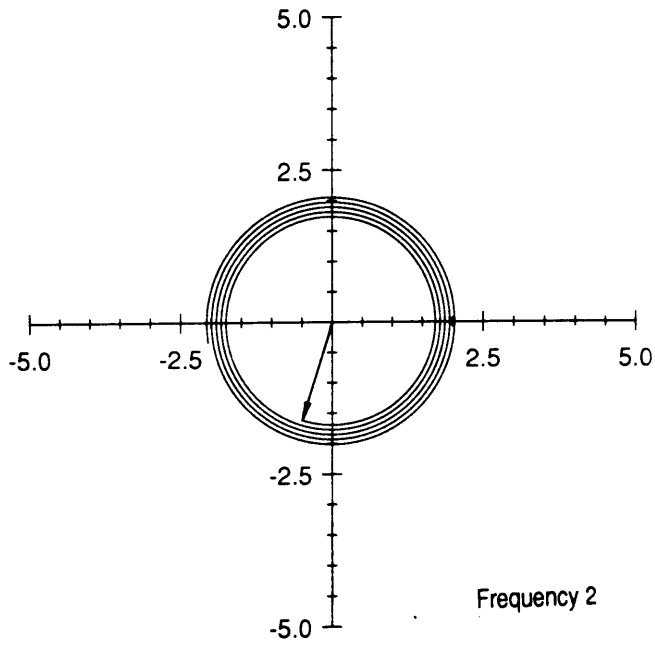
Figure 9. Difference vector plot for both frequencies for Simulation 1.

rate as shown in figure 10. By integrating the burn rate and comparing the result with the initial web thickness, the correct value for the propellant wavelength can be found. This can be done by adjusting the value of λ_p until the integrated burn rate equals the initial web thickness. The correct burn rate arrived at by this means is illustrated in figure 11.

FREQUENCY 2
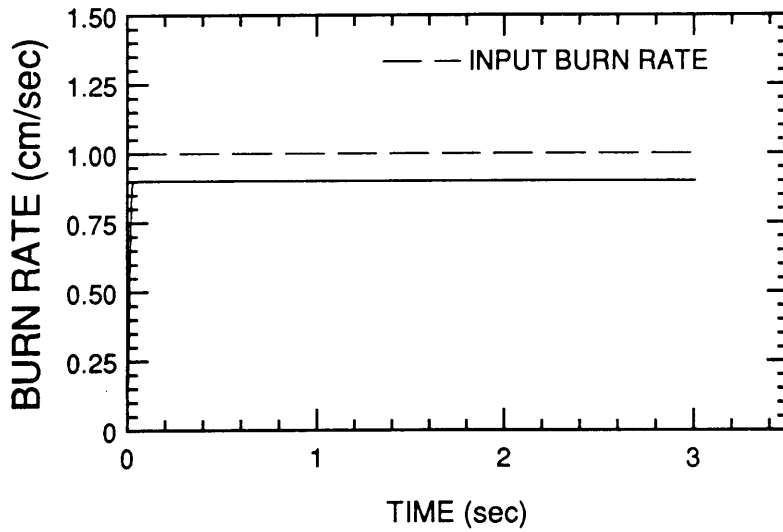
FREQUENCY 1
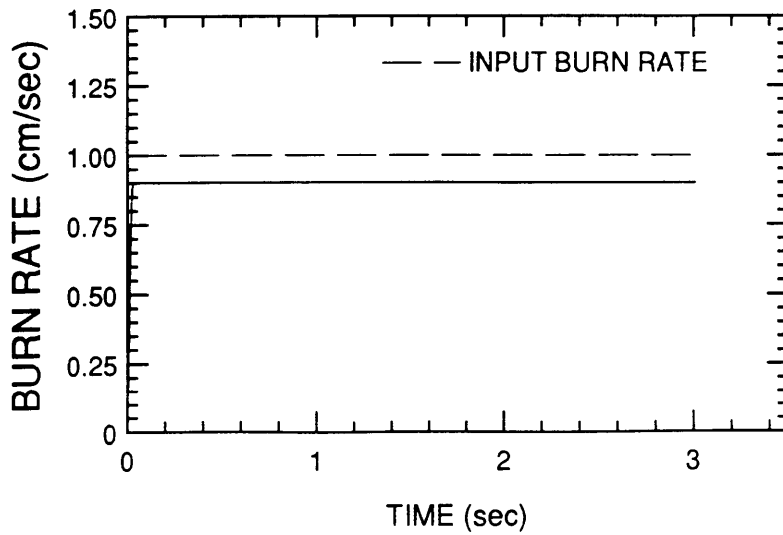
Figure 10. Burn rate curves for Simulation 1.
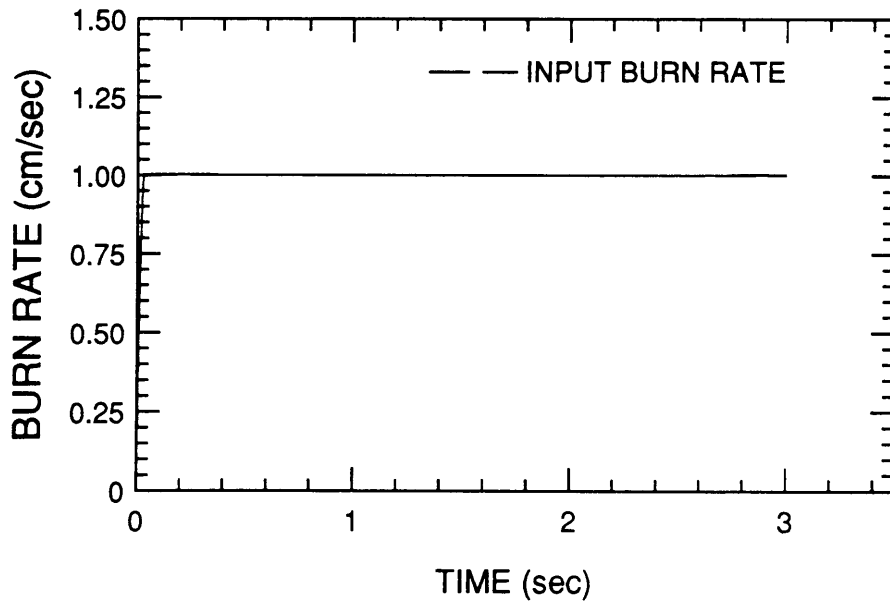
Figure 11. Integration corrected burn rate curve for Simulation 1.

3.2.2 Simulation 2

The second simulation is of a variable burn rate with an initial burn rate of 1.0 cm/sec increasing to 1.25 cm/sec by the end of the burn. The web thickness is 3.375 cm with a total burn time again, of three seconds. Table 2 contains the simulation parameters. In this simulation, a second moving reflection was added which represents a reflection from a fixed surface opposite the burning surface. This type of reflection has a rate of phase change given by equation 2.12, and is described in section 2.2. Using a wavelength ratio of 0.43 for propellant-to-combustion chamber, the rate of phase change of this vector (using equation 2.11) is 57 percent of the burning surface vectors rate of phase change.

The effect of the third vector is seen in the total vector plots for both frequencies in figure 12. Here the vectors do not constantly increase in magnitude, but both increase and decrease, resulting in crossover points in the plot. Plots of the difference vectors (figure 13) show similar effects with the erratic magnitudes leading to variations in the rate of phase change. There is also a general increase in magnitude of the vectors which occurs as the burn rate increases with time.

The burn rate plots (figure 14) follow the input burn rate but oscillate, resulting in burn rate errors for both curves of up to 20 %. However, the oscillations are out of phase and frequency. The time rate of phase change for each frequency signal was adjusted until the ratios of each signals phase change matched the frequency ratio of the frequencies used. This technique comes from equation 2.5 of section 2.1. This results in the composite burn rate curve shown in figure 15. Here the error has been reduced to less than 5 %. This error reduction depends upon the secondary burn rate oscillations being offset, which in turn depends upon the initial rocket motor geometry. The frequency separation of the frequencies being used is also a factor in the ability of the system to eliminate errors.

Table 2. Simulation 2 parameters.

Frequency 1 (Ghz):	9.20
Frequency 2 (Ghz):	10.45
Power Ratio (1/2):	1.0

Vector Magnitudes (mV) for Frequency 1:

V_a:	8.0
$V_b(t)$:	20.0 increasing to 24.6
$V_r(t)$:	8.0 increasing to 9.86

Vector Rotation Rates (rad/sec) for Frequency 1:

V_a:	fixed
$V_b(t)$:	8.925 increasing to 9.856
$V_r(t)$:	5.08 increasing to 6.35

Vector Initial Angles (deg):

V_{a1}:	0.0	V_{a2}:	60.0
$V_{b1}(t)$:	286.0	$V_{b2}(t)$:	325.0
$V_{r1}(t)$:	146.0	$V_{r2}(t)$:	57.0

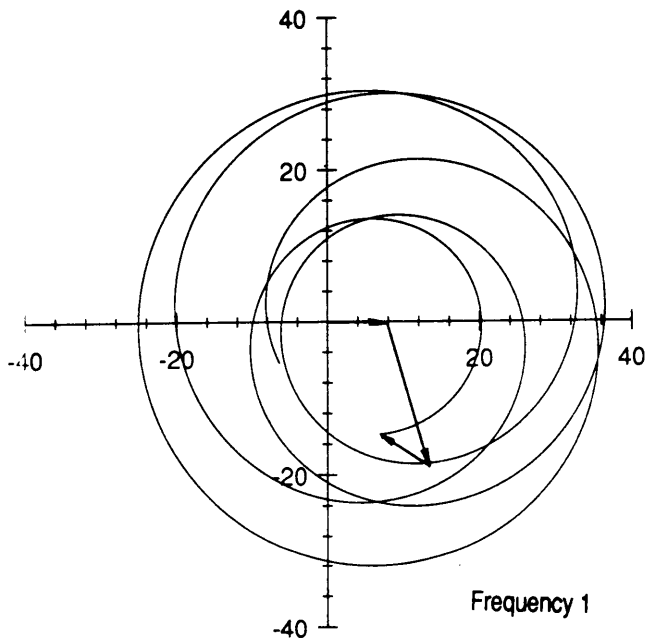|	
Input Wavelength, Frequency 1 (cm):	1.408
Propellant Web Thickness (cm):	3.375
Simulated Burn Rate (cm/sec):	1.0 increasing to 1.25
Burn Time (sec):	3.0

Figure 12. Total vector plots for both frequencies for Simulation 2.
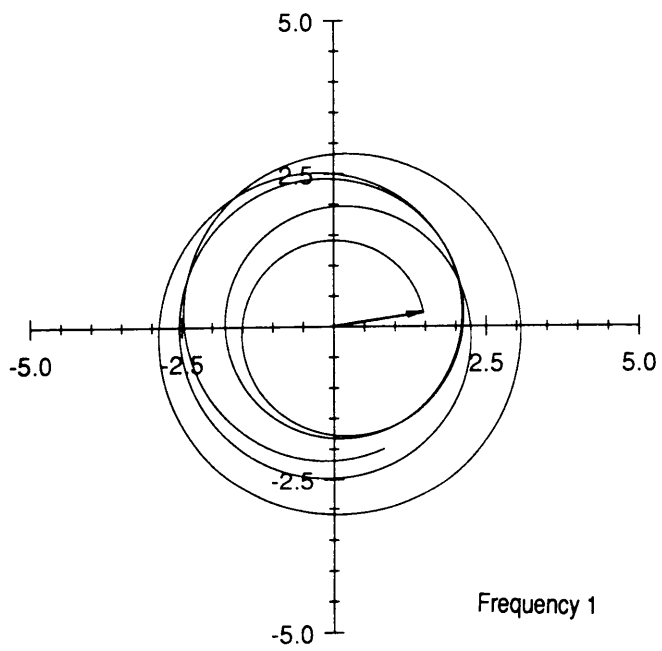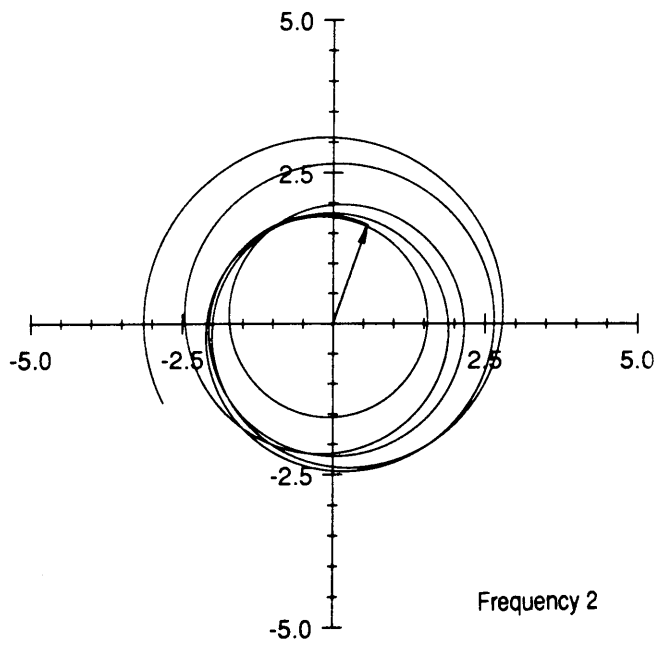
Figure 13. Difference vector plot for both frequencies for Simulation 2.

Figure 14. Burn rate curves for Simulation 2.
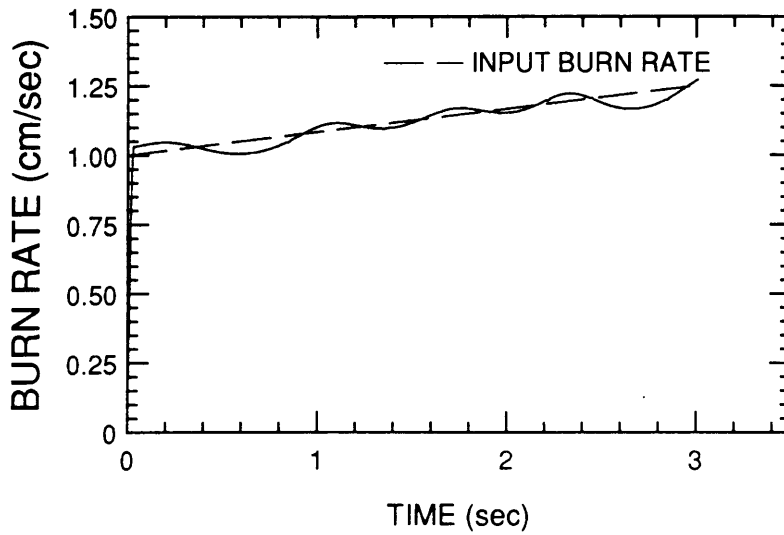
Figure 15. Composite burn rate curve for Simulation 2.

3.2.3 Simulation 3 and 4

The next two simulations are included in one section to provide a comparison of a variation in the frequency ratios. Simulation 3 uses frequencies of 8.5 and 11.5 Ghz while simulation 4 uses 9.2 and 10.45 Ghz. This corresponds to a frequency ratio variance of approximately 30%. Both are three vector simulations with one fixed and two moving vectors. The second moving vector is again a secondary reflection off the far surface of the combustion chamber. The burn rate is 1.0 cm/sec and initial vector angles are such that the burn rate oscillations are close in alignment. Table 3 contains the parameters for both simulations.

Since these simulations are similar to simulation 2, only the burn rate curves are presented. Figure 16 shows the burn rate curves for simulation 3. Here the peaks of the oscillations start out close together but the frequency variance of the signals causes later peaks to be offset. In the composite burn rate curve (figure 17), the error has been reduced from a previous maximum of 20% to no more than 15%. Although not as significant as the previous reduction to 5% in simulation 2, it is still a 25% error reduction. In contrast, figure 18 shows the burn rate curves for simulation 4. The oscillations in burn rate are closely aligned throughout the burn due to the smaller frequency separation. The error reduction in the composite burn rate curve (figure 19) is therefore nil.

Table 3. Simulation 3 and 4 parameters.

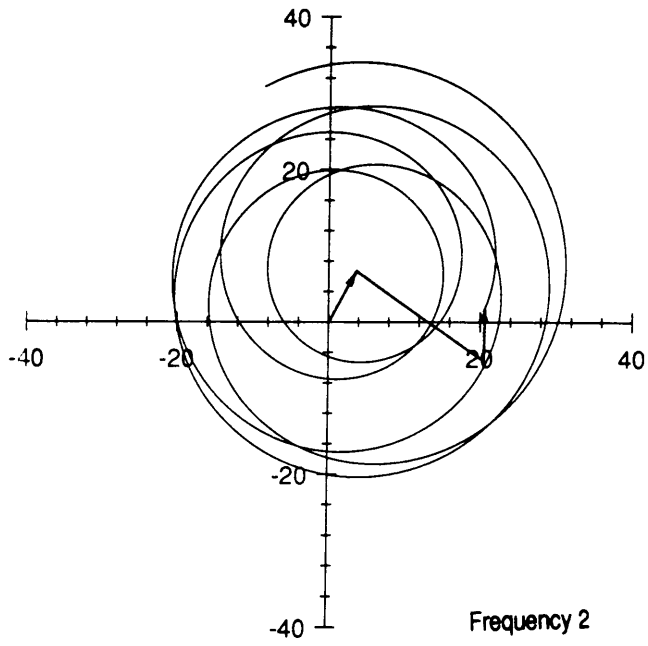| Simulation:	3	4
Frequency 1 (Ghz):	8.50	9.20
Frequency 2 (Ghz):	11.5	10.45
Power Ratio (1/2):	1.1	1.1
Vector Magnitudes (mV) for Frequency 1:		
V_a:	10.0	10.0
$V_b(t)$:	20.0 incr. to 24.6	20.0 incr. to 24.6
$V_r(t)$:	10.0 incr. to 12.3	10.0 incr. to 12.3
Vector Rotation Rates (rad/sec) for Frequency 1:		
V_a:	fixed	fixed
$V_b(t)$:	8.246	8.925
$V_r(t)$:	4.693	5.08
Vector Initial Angles (deg):		
V_{a1}:	0.0	0.0
$V_{b1}(t)$:	60.0	94.0
$V_{r1}(t)$:	280.0	36.0
V_{a2}:	60.0	60.0
$V_{b2}(t)$:	220.0	2.0
$V_{r2}(t)$:	160.0	335.0
Input Wavelength, Frequency 1 (cm):	1.524	1.408
Propellant Web Thickness (cm):	3.0	
Simulated Burn Rate (cm/sec):	1.0	
Burn Time (sec):	3.0	

FREQUENCY 2

FREQUENCY 1
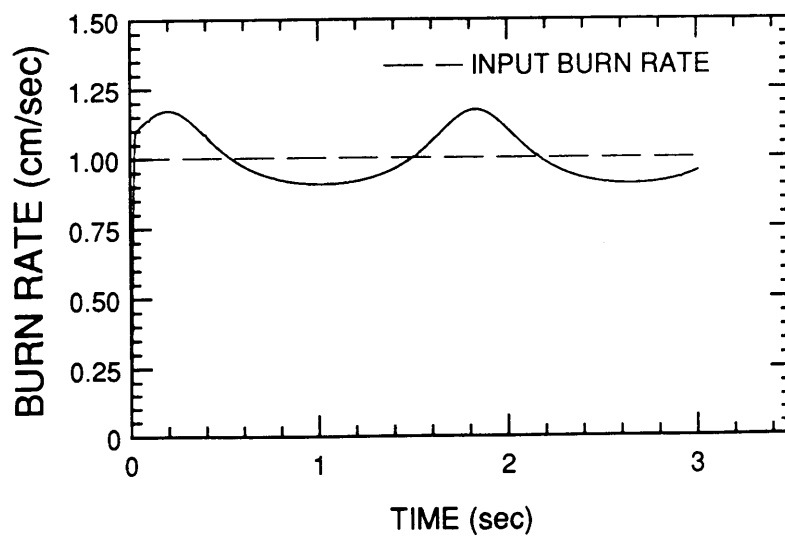
Figure 16. Burn rate curves for Simulation 3.
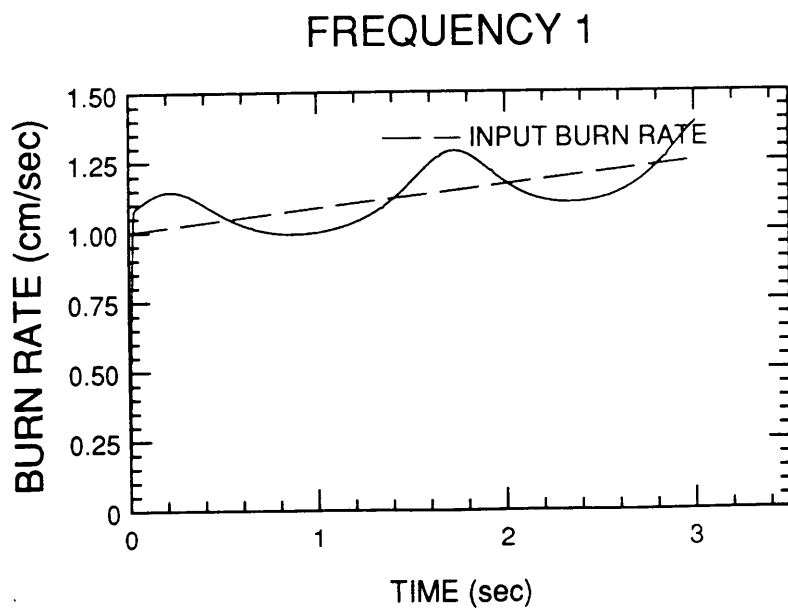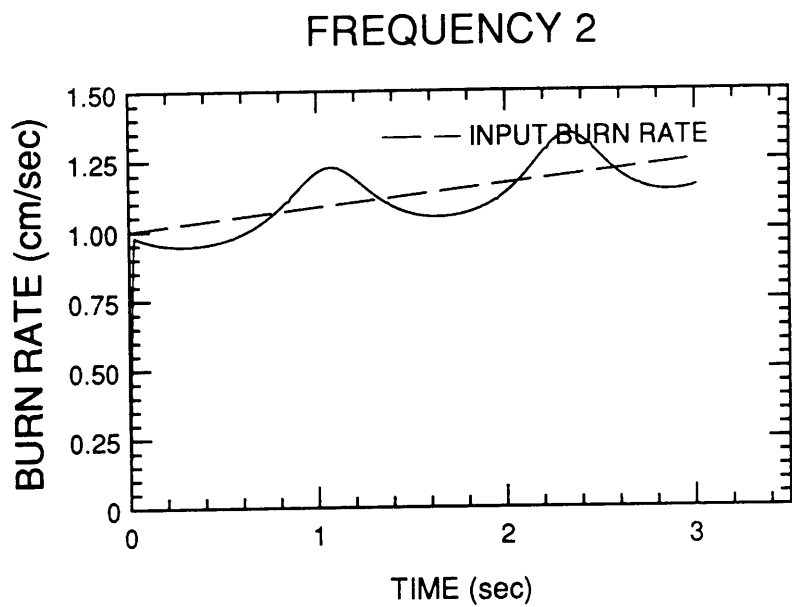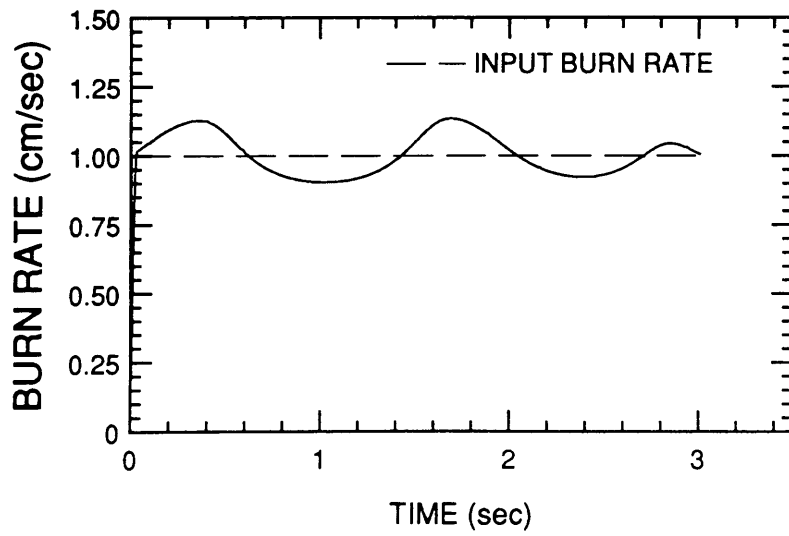
Figure 17. Composite burn rate curve for Simulation 3.
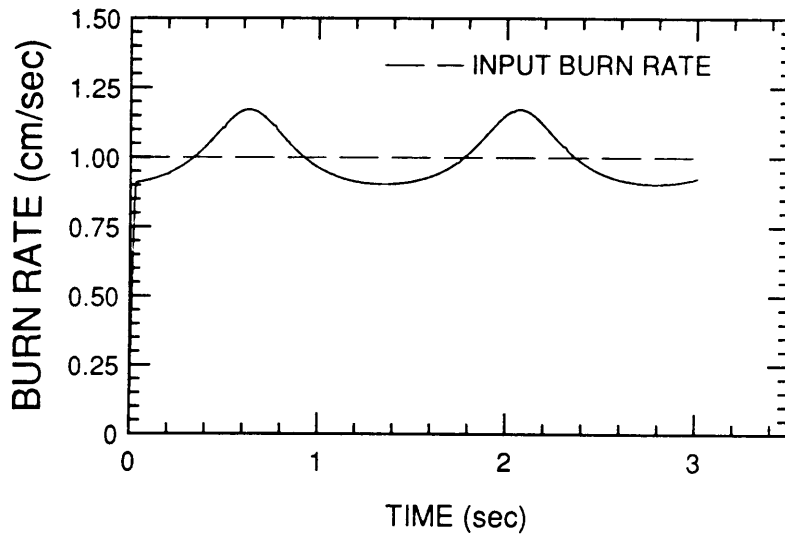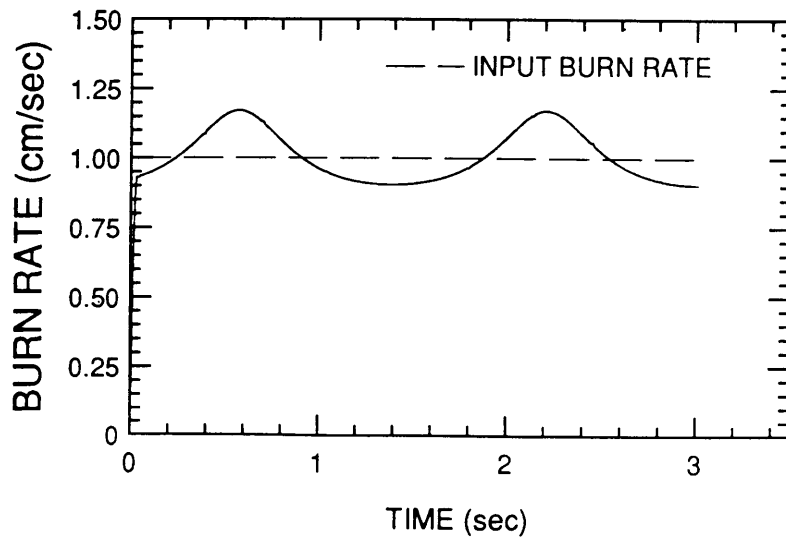
Figure 18. Burn rate curves for Simulation 4.
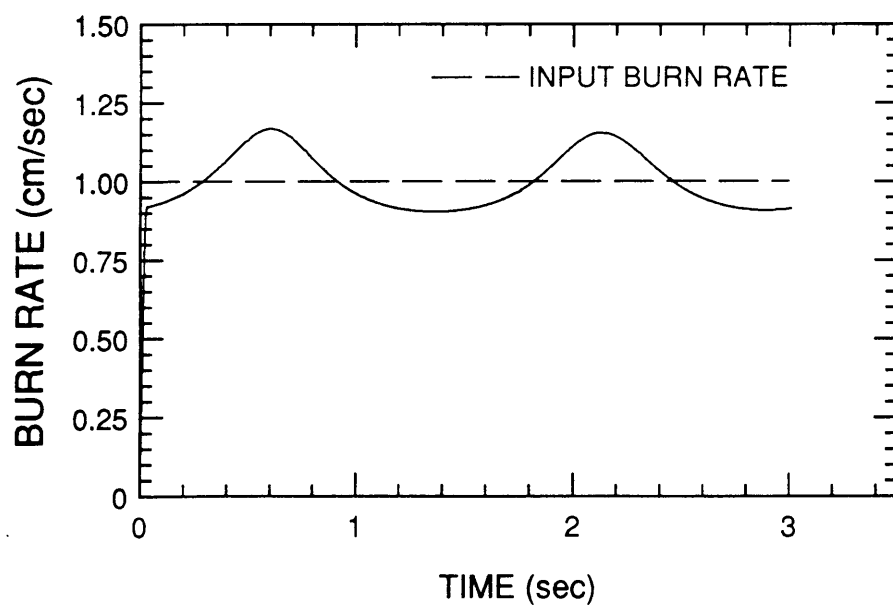
Figure 19. Composite burn rate curve for Simulation 4.

3.2.4 Simulation 5

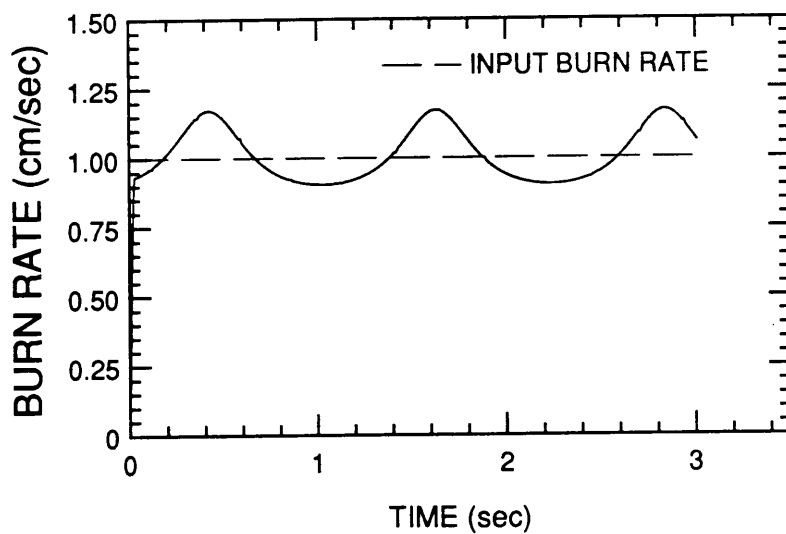Simulation 5 examines the effect of a secondary reflection in the propellant. This reflection has travelled through the propellant four times and is initially 0.10 times the size of the burning surface vector. It is rotating at twice the rate of the burning surface vector and increases in magnitude at a much higher rate. Table 4 contains the complete simulation parameters.

Plots of the total vector magnitude and phase (figure 20) show a surprising symmetry. The plot for frequency 1 has overall a higher magnitude and smaller absolute phase change due to its corresponding higher power and lower frequency. Neither plot shows any crossing points due to magnitude oscillations, but there is a magnitude contraction in each plot which occurs at the same phase and corresponds to the moving vectors being 180 degrees opposed initially.

The magnitude contractions also show up in the difference vector plots in figure 21. Here a magnitude contraction occurs for each plot at a single phase angle. For frequency 1, the contraction is at around 240 degrees and at 135 degrees for frequency 2. This leads to the burn rate curves shown in figure 22. The oscillations in burn rate are offset due to the offset of the magnitude contractions in the difference vector plots. The burn rate oscillations themselves (caused by the magnitude contractions) result in errors of greater than 50% of the input burn rate. These oscillations also increase in magnitude over time with the increase in magnitude of the secondary vector.

The plot of the composite burn rate is shown in figure 23. Error reduction occurs only in the initial stages of the burn, leaving large errors during the rest of the burn. Clearly, a larger frequency separation (such as in simulation 3) would reduce the error to a greater degree. To confirm this, such a simulation was done with frequencies of 8.5 and 11.5 Ghz. All other parameters were maintained with the exception of initial vector

Table 4. Simulation 5 parameters.

Frequency 1 (Ghz):	9.20		
Frequency 2 (Ghz):	10.45		
Power Ratio (1/2):	1.0		

Vector Magnitudes (mV) for Frequency 1:

V_a:	10.0		
$V_b(t)$:	20.0 increasing to 24.6		
$V_r(t)$:	2.0 increasing to 4.6		

Vector Rotation Rates (rad/sec) for Frequency 1:

V_a:	fixed		
$V_b(t)$:	8.925		
$V_r(t)$:	17.85		

Vector Initial Angles (deg):

V_{a1}:	0.0	V_{a2}:	0.0
$V_{b1}(t)$:	60.0	$V_{b2}(t)$:	302.0
$V_{r1}(t)$:	154.0	$V_{r2}(t)$:	245.0

|	
Input Wavelength, Frequency 1 (cm):	1.408
Propellant Web Thickness (cm):	3.0
Simulated Burn Rate (cm/sec):	1.0
Burn Time (sec):	3.0
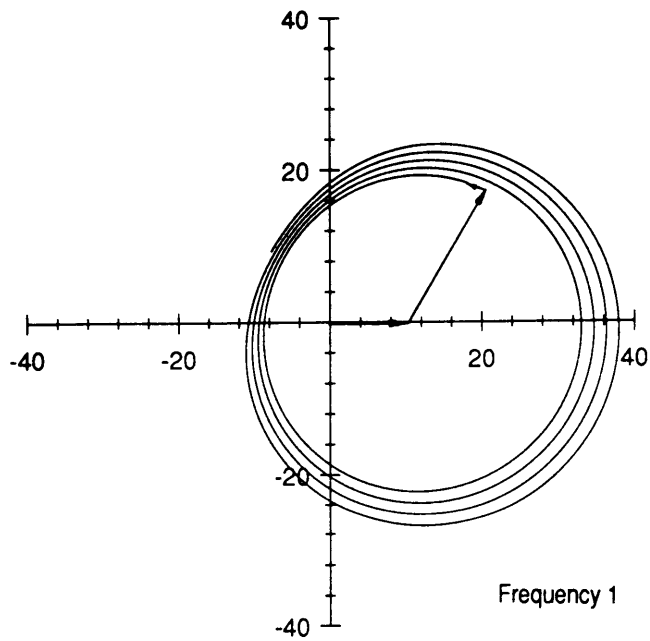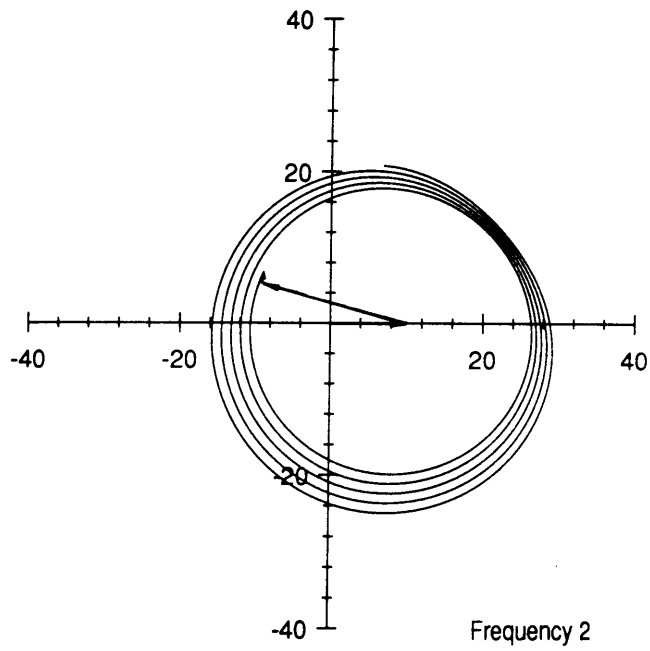
Figure 20. Total vector plots for both frequencies for Simulation 5.

Figure 21. Difference vector plot for both frequencies for Simulation 5.
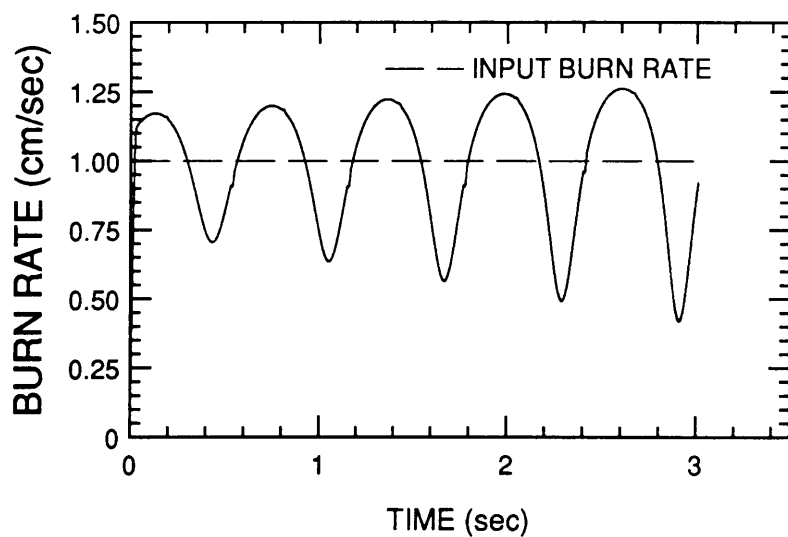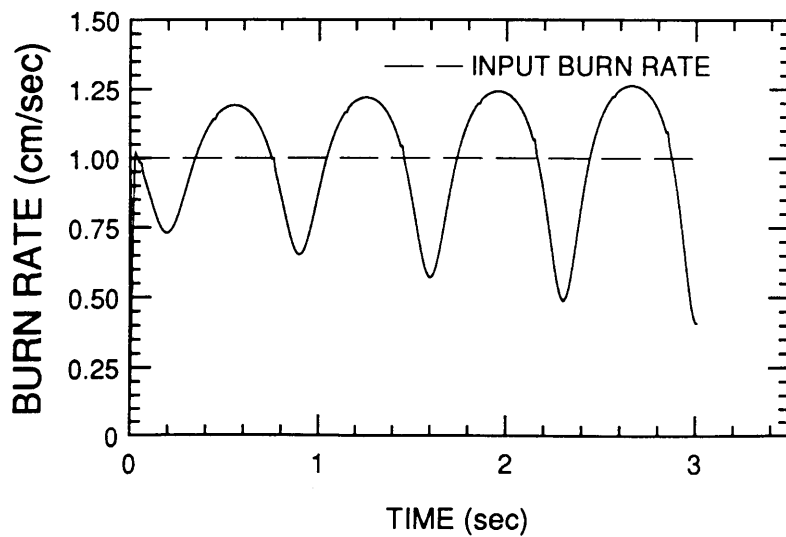
Figure 22. Burn rate curves for Simulation 5.

Figure 23. Composite burn rate curve for Simulation 5.

angles which changed due to the frequency change. Figure 24 contains the burn rate plots which again show large oscillations resulting in errors of greater than 50%. The oscillations are also more closely spaced for the high frequency (Ghz) and further apart for the lower frequency signal (8.5 Ghz). In Figure 25 the error for this simulation has been reduced to less than 25% except for one oscillation which occurs at 1.25 seconds burn time.

FREQUENCY 2

FREQUENCY 1
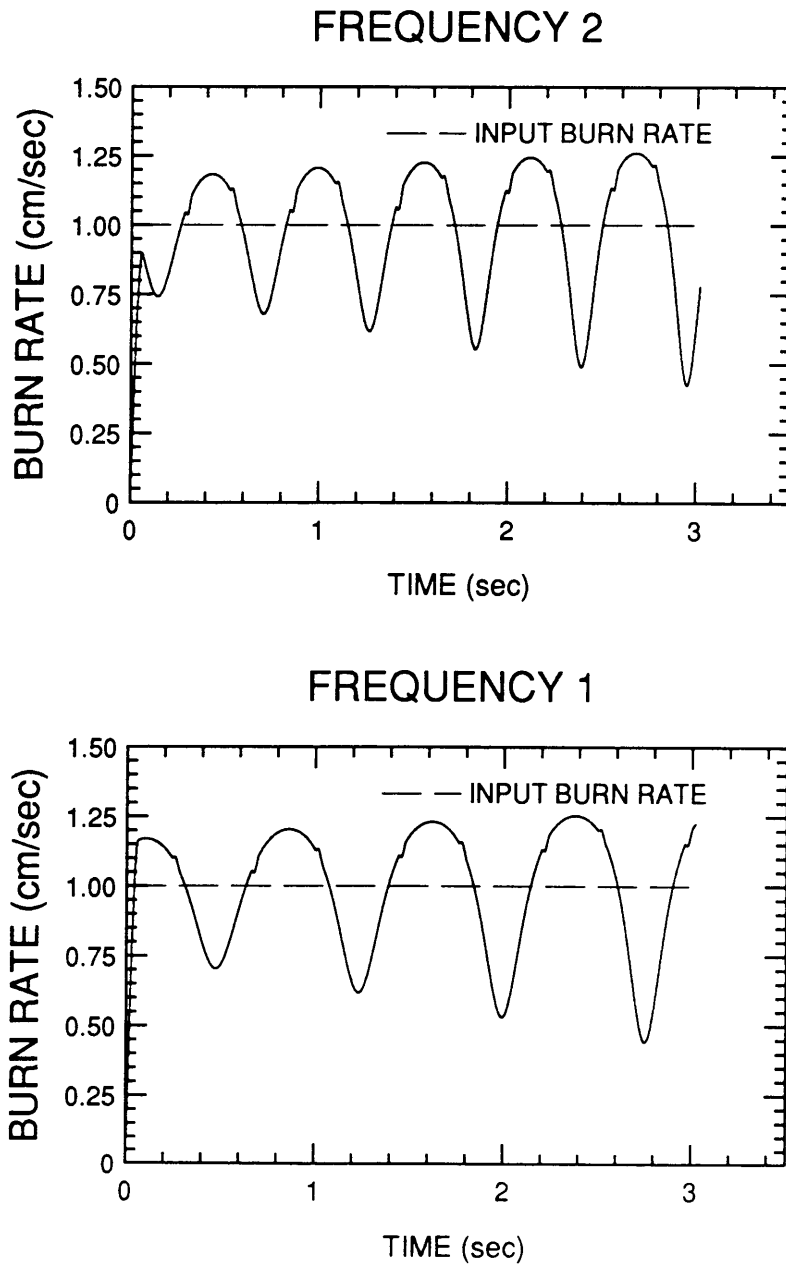
Figure 24. Burn rate curves for Simulation 5 at 8.5 and 11.5 Ghz.
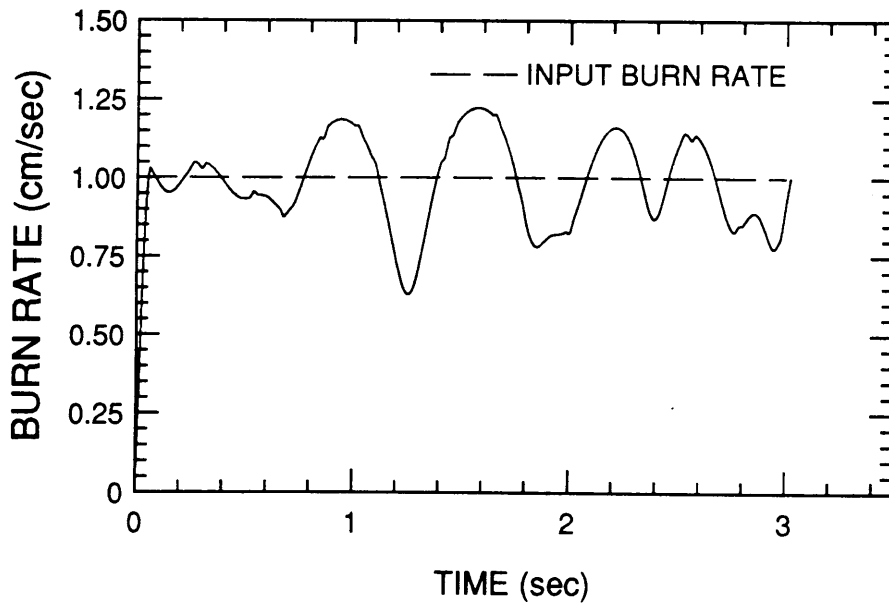
Figure 25. Composite burn rate curve for Simulation 5 at 8.5 and 11.5 Ghz.

3.2.5 Simulation 6

Simulation 6 gives an idea of the effect a small, quickly rotating vector has on the burn rate. The second moving vector simulates a reflection which traverses the propellant web six times, giving it a rate of phase change three times that of the burning surface vector. The magnitude ratio of V_r/V_c is only 0.015 (Complete simulation parameters are given in table 5). Such a small vector is not clearly visible in the total vector plots of figure 26. These plots show distinct magnitude contractions due to the second moving vector. Each plot has two magnitude contractions which are directly opposed. The difference vector plots are similar (figure 27), with more distinct magnitude contractions again appearing 180 degrees apart. The burn rate curves resulting from this simulation (figure 28) contain oscillations of a higher frequency than previously seen, but with less absolute error (approximately 25%). The error reduction achieved in this simulation is limited, with the error being reduced only in the second quarter of the burn rate curve as seen in figure 29.

3.3   Discussion of Results

Overall, the simulations show some of the advantages and some of the limitations of the two frequency system if the assumptions made are reasonable. The error reduction possible appears limited by the frequency separation and initial motor geometry. Simulation 1 showed the dramatic error reduction that could occur for a slow moving secondary reflection and geometry where these reflections from each frequency are offset. In later simulations (5 and 6), reflections that rotate at a higher rate than the burning surface vector result in larger errors which are much more immune to the error reduction available using two frequencies, though some error reduction can be achieved. More advanced data reduction could overcome these limitations. The use of a higher frequency separation will also improve the error reduction for all types of reflections

(simulations 3,4, and 5). For the simple data reduction techniques used, the two frequency system should provide improved accuracy in some cases, with little increase in complexity, as the next chapter on hardware demonstrates.

Table 5. Simulation 6 parameters.

Frequency 1 (Ghz):	9.20
Frequency 2 (Ghz):	10.45
Power Ratio (1/2):	1.2

Vector Magnitudes (mV) for Frequency 1:

V_a:	10.0
$V_b(t)$:	20.0 increasing to 24.6
$V_r(t)$:	0.3 increasing to 1.05

Vector Rotation Rates (rad/sec) for Frequency 1:

V_a:	fixed
$V_b(t)$:	8.925
$V_r(t)$:	26.775

Vector Initial Angles (deg):

V_{a1}:	0.0	V_{a2}:	0.0
$V_{b1}(t)$:	60.0	$V_{b2}(t)$:	164.0
$V_{r1}(t)$:	231.0	$V_{r2}(t)$:	340.0

|	
Input Wavelength, Frequency 1 (cm):	1.408
Propellant Web Thickness (cm):	3.0
Simulated Burn Rate (cm/sec):	1.0
Burn Time (sec):	3.0
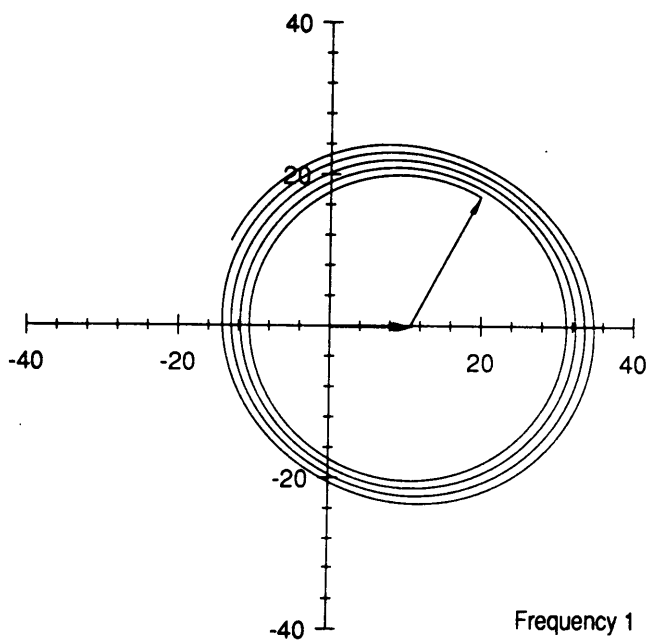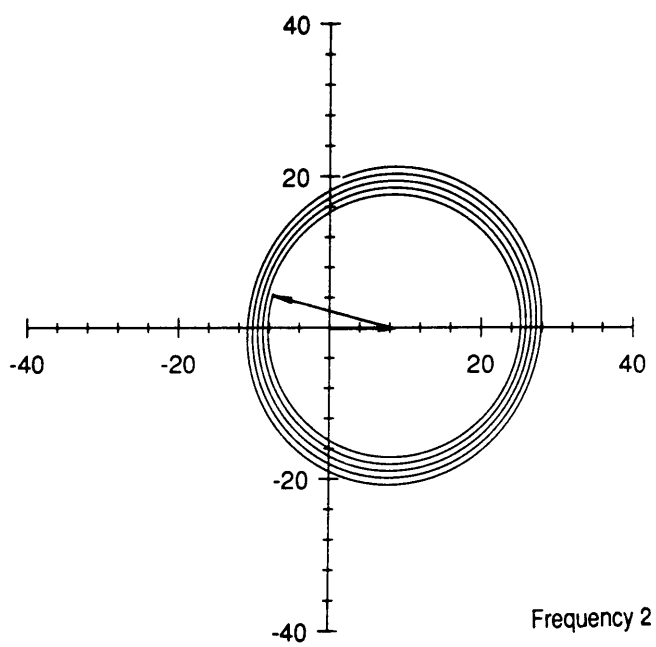
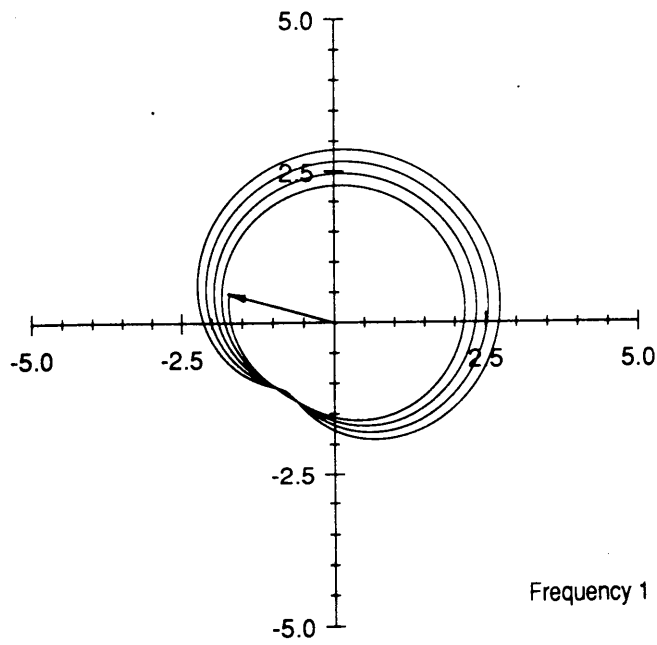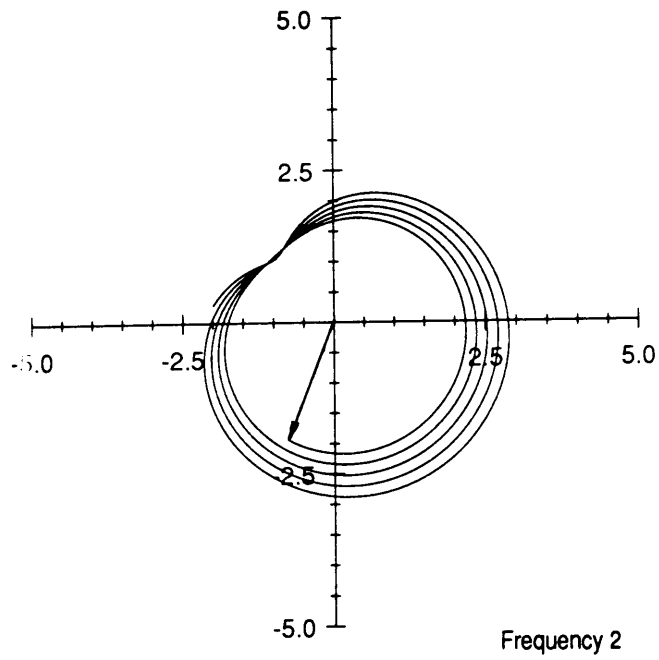Figure 26. Total vector plots for both frequencies for Simulation 6.
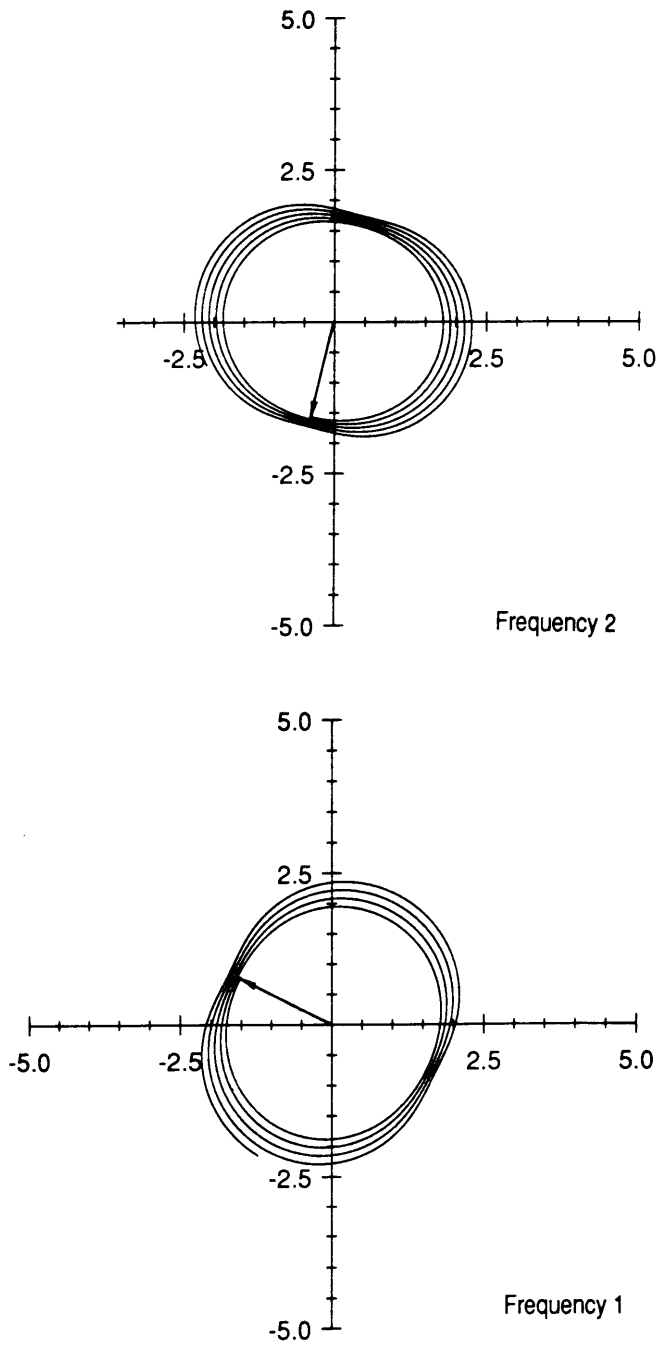
Figure 27. Difference vector plot for both frequencies for Simulation 6.

FREQUENCY 2
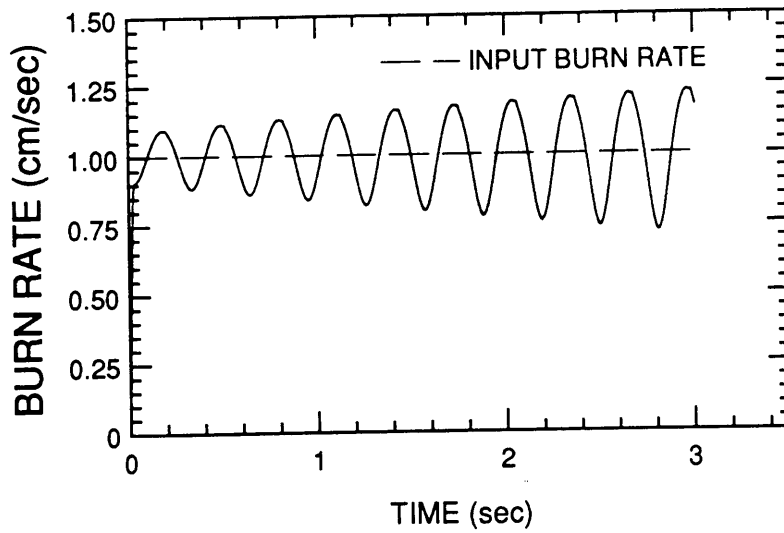
FREQUENCY 1
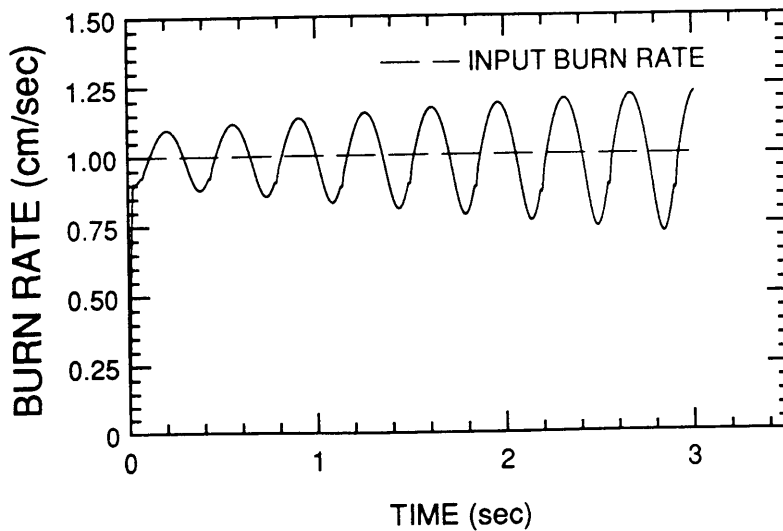
Figure 28. Burn rate curves for Simulation 6.
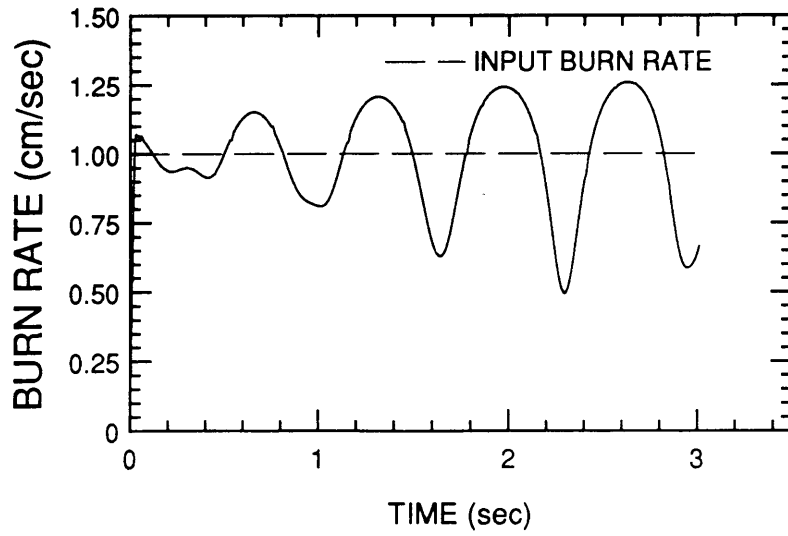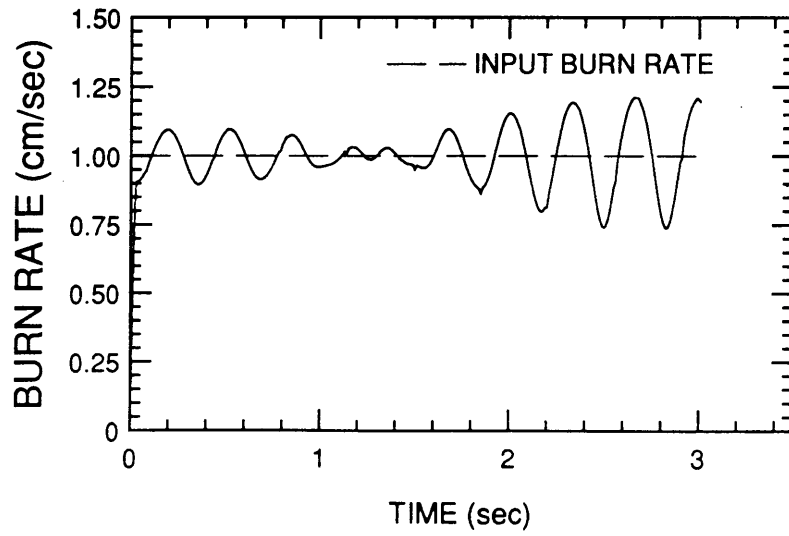
Figure 29. Composite burn rate curve for Simulation 6.

4. SYSTEM HARDWARE AND INSTRUMENTATION

Once the modeling of the microwave behavior has been done, the system which delivers and measures the microwaves to the rocket motor must be developed. Much of the hardware of the present system was taken from the earlier, single frequency system. However, major changes needed to be made to the single frequency system. These changes consisted of developing a system which could simultaneously transmit two microwave frequencies to the same measurement point while still being able to measure each signal separately.

In addition to these basic hardware changes, the use of two frequencies required new instrumentation to enable measurement of the signals. The previous system used a phase-gain indicator which took reference and test signal inputs and output the phase and magnitude difference between them. A high speed digital oscilloscope was acquired which allowed measurement of four signals and proved to be an excellent diagnostic tool for determining the behavior of two frequencies in the test equipment. The new instrumentation and measurement technique also required development of new software which is described in later sections. In spite of these advantages, the oscilloscope was not able to acquire data at a rate fast enough to support a full scale test. Nonetheless, the system is described and limited test results are presented in chapter 5 which prove the viability of the design.

4.1   Microwave Measurement System

A schematic of the measurement system (minus the peripheral data acquisition system) is shown in figure 30.

Microwave radiation is generated by the two Gunn diode microwave oscillators. These are modified C-2070 units made by MPD, Inc. Figure 31 is a diagram of the oscillators showing electrical connections and other features. Both oscillators produce approximately 100 mW of microwave energy with a 10 volt DC input and draw 300 mA of current. The oscillators are set for 9.15 GHz and 10.45 GHz. Each is adjustable over a range of +/- 0.25 GHz through use of a self-locking screw on the unit. This screw adjusts the frequency by altering the oscillator's cavity dimensions. A 10 microfarad capacitor is wired across the electrical leads to provide voltage spike protection.

Two reference signals are extracted from the main signals through two 20 dB waveguide couplers. These couplers are WR-62 sections (as are all the waveguide sections and components) which are sized for transmission of X-band radiation (8.2-12.4 GHz). A 3 dB coupler is used to couple the two main signals, allowing use of common waveguide sections and one microwave horn. After exiting the 3 dB coupler the combined signal passes through an isolator (to prevent unwanted reflections from reaching the preceding section) and a precision variable attenuator which allows control of the microwave power level leaving the horn.

Radiation through the horn is reflected off the combustion chamber/propellant interface after passing through the rocket motor casing and insulation (figure 32). An E-H tuner (a straight waveguide section with two 90 degree adjustable shorts) is used to zero out, or dampen, the reflections off the motor casing and other fixed material interfaces by creating a similar reflection 180 degrees out of phase.

MICROWAVE MEASUREMENT SYSTEM (MMS)
(DUAL FREQUENCY)
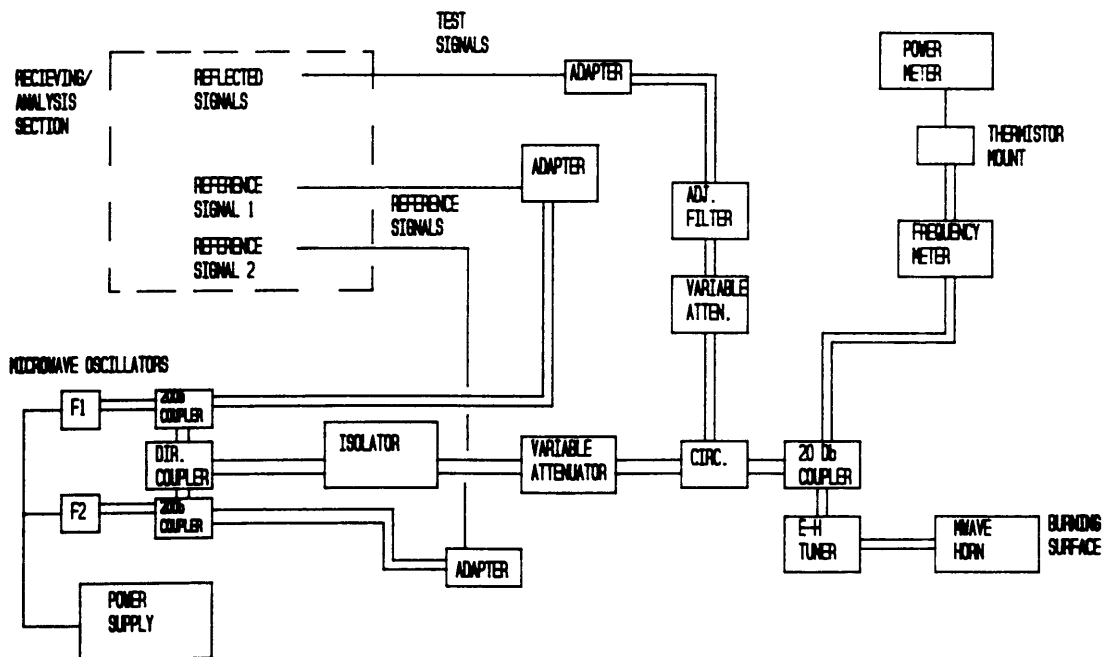
Figure 30. Dual frequency microwave measurement system.
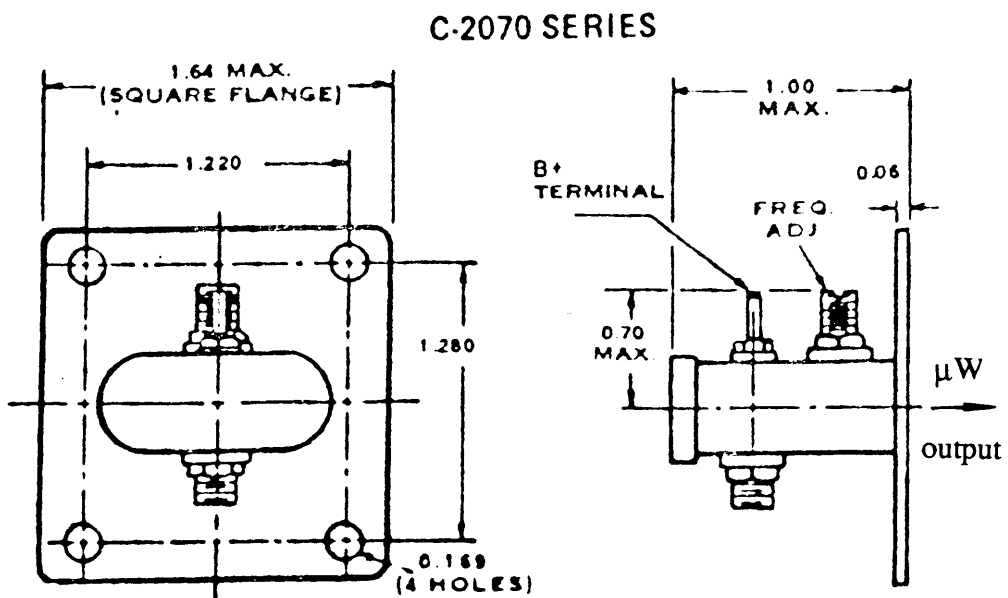
Figure 31. Schematic of C-2070 microwave oscillator.
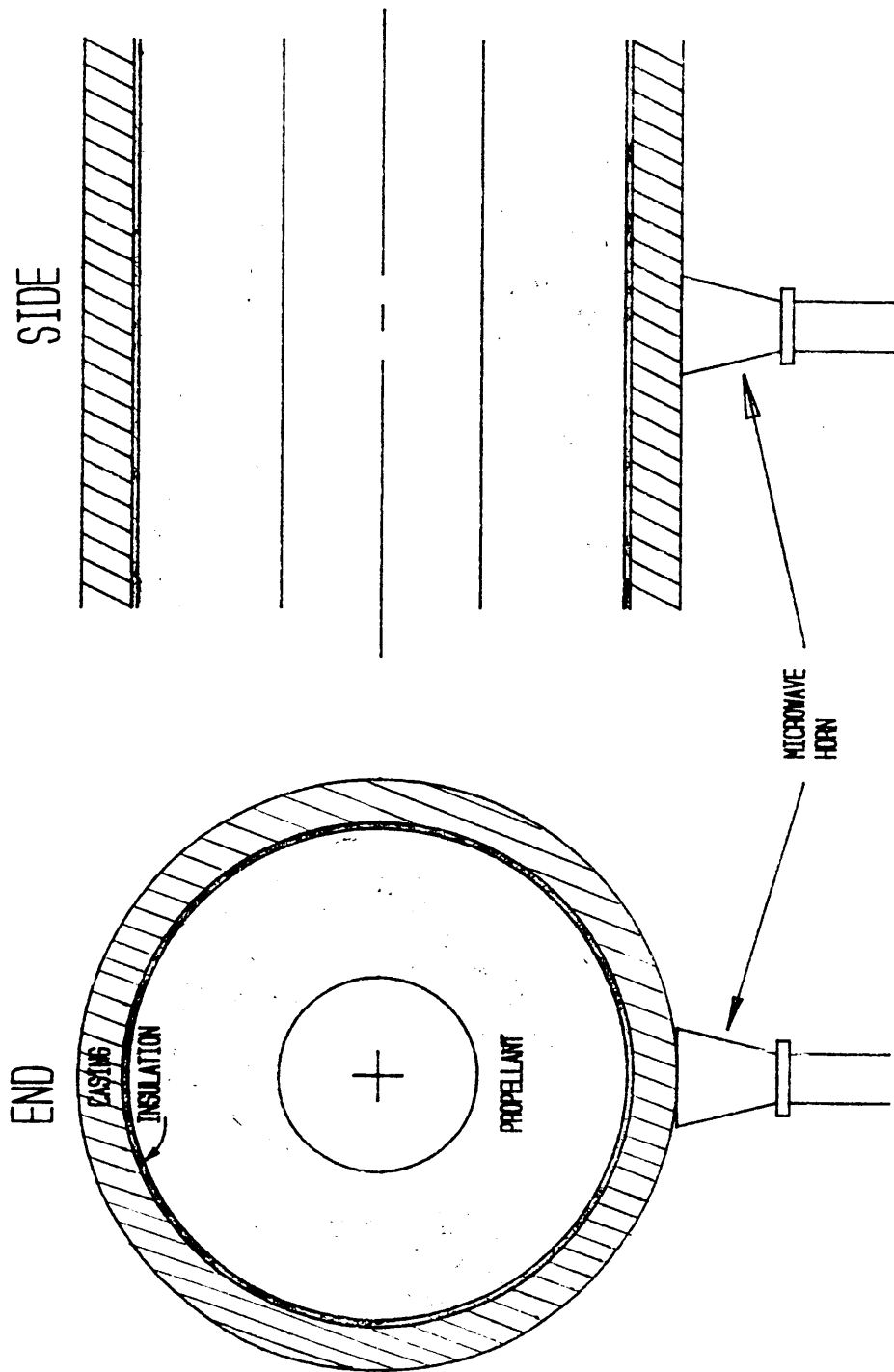
Figure 32. Microwave horn and rocket motor cross section.

The circulator is used to route the reflected signals into the receiving section of the measurement system. The combined signal is passed through a variable attenuator, an isolator, and an adjustable waveguide short section to the coaxial cable adapter. The attenuator controls the total power of the combined reflected signal while the adjustable short is used to vary the power of the individual frequencies by acting as an adjustable filter. This is to ensure that one frequency does not dominate the system. The isolator acts against any stray reflections due to the filter.

Coaxial cable adapters are used on both reference signal pickups in addition to the combined reflected signal pickup. These three signals carry the relevant information to the test instrumentation.

4.2   Test and Analysis Section

The test and analysis section consists of four major components. These are the data acquisition computer, the digital oscilloscope, the 4-channel test set, and the trigger signal generator. These instruments and their interfaces are shown in figure 33.

Waveguide-to-coaxial cable adapters are used on the reflected signal output and reference signal outputs. N-to-SMA adapters are used with the coaxial adapters and 50-ohm double-shielded coaxial cables to feed the signals into the HP 54121A 4-channel test set. Reference signals for frequency 1 (9.20 GHz) are input to channel 2. Channel 3 carries the reference signals for frequency 2 (10.45 GHz). The combined reflected signal is fed through a two-way power splitter with one output going to the test set (channel 4) and the second to the HP 54118A trigger signal generator.

The trigger signal generator puts out a 5-20 KHz trigger signal which is synchronized with the microwave signal input from channel 4. This trigger signal is input to the test set and allows the coherent viewing of the three microwave signals on the screen.
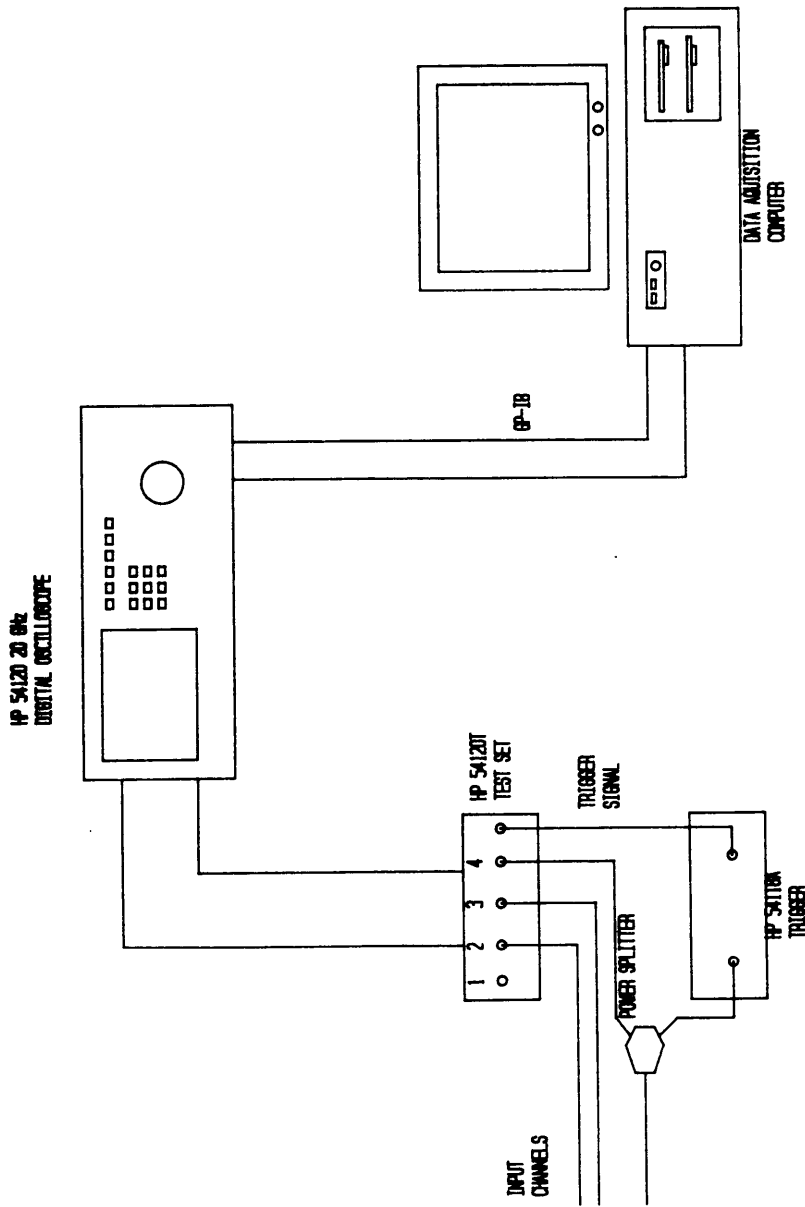
Figure 33. Instrumentation and data acquisition setup.

Since the trigger signal input (and channel 4) is a combined signal of two frequencies, triggering allows both frequency 1 and frequency 2 to be viewed. The adjustable filter described in section 3.1 is used to ensure that channel 4 is an equal combination of both frequencies. If one frequency is dominant, the trigger signal becomes synchronized with just that one frequency, resulting in loss of the second frequency.

Figure 34 is a plot of the oscilloscope screen showing the three input signals. Channel one is blank, while channels two and three contain the waveforms for the two frequencies. Channel four, the combined signal, varies in amplitude and frequency--the result of combining two signals with different frequencies.

The HP 54120 digital oscilloscope is equipped with a waveform save feature which allows storing and recall of data on the screen. However, only four screens of data can be stored, which is less than the amount of data that is recorded in a standard test. This necessitates the use of a peripheral data storage and control system.

The HP 54120 digital oscilloscope is equipped with a GP-IB standard interface for data transfer and control. An IBM-AT based computer with a GP-IB adapter card and hard disk is used for acquisition of data from the oscilloscope and later for post-acquisition manipulation. A BASIC software program (given in Appendix B) is used for control of the oscilloscope and routing of data to the hard disk in the computer. The data acquisition computer is an 80286-based machine equipped with two floppy disk drives (3.5 in and 5.25 in) and two hard disks (20 MB and 40 MB). Data manipulation programs are resident in the 20 MB hard disk or can be loaded through one of the floppy disk drives. Test data is sent to files in the 20 MB drive. This type of architecture allows for quick manipulation of test data and display of results.

Ch. 2   =   320.0 ∎Volts/div   Offset   =   0.000   Volts
Ch. 3   =   320.0 ∎Volts/div   Offset   =   0.000   Volts
Ch. 4   =   320.0 ∎Volts/div   Offset   =   0.000   Volts
Timebase =   100 ps/div   Delay   =   16.0000 ns
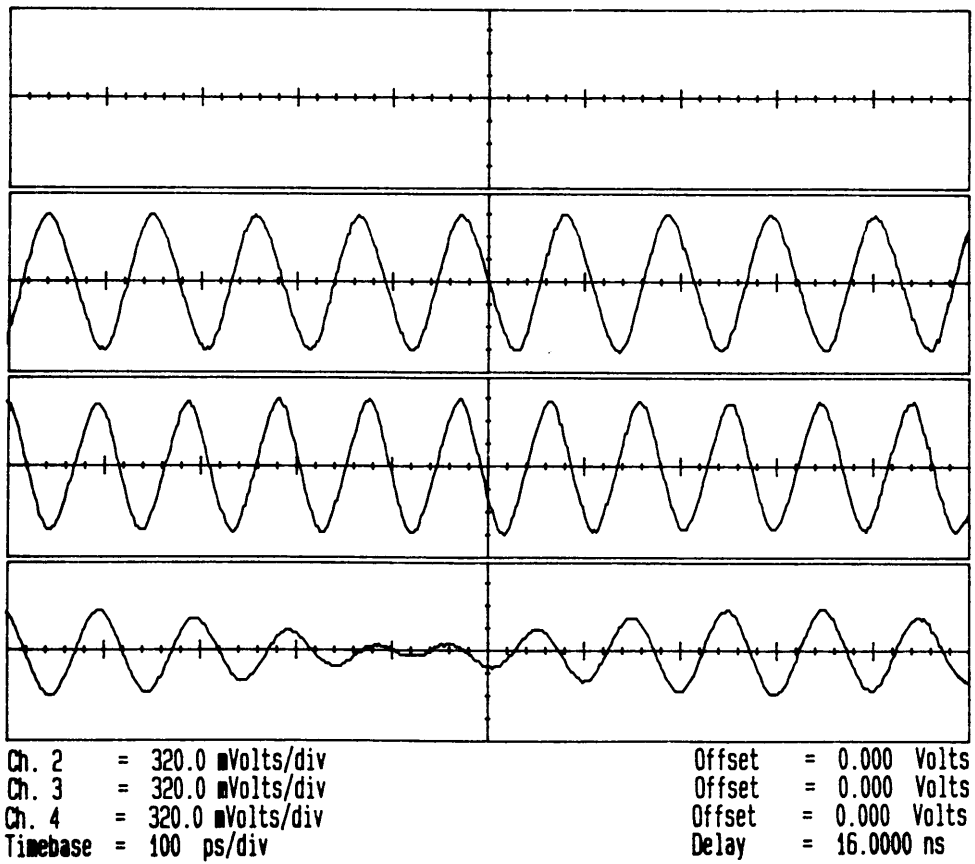
Figure 34. Screen display of oscilloscope with three channels displayed.

The test instrumentation set-up was designed to provide both a diagnostic capability to the system and a quick and easy method for gathering test data. The digital oscilloscope allows the viewing of the microwaves at various points in the system to better assess the system's performance. The data acquisition system allows easy access to and manipulation of data generated during testing.

The following section describes in further detail the functioning of the controlling programs in the computer and the features present in the oscilloscope.

4.3   Data Acquisition and Manipulation

The major objective of the data acquisition system is the accurate recording of phase change data for the two frequencies being used. This phase change data occurs in the reflected signals which are also used (while still combined as one signal) as the trigger signal input. Because of this, channel four, the combined signal, shows no phase change when the reflected signals are in fact changing in phase during a test. However, the two reference signals (channels two and three) appear to change in phase on the oscilloscope as the trigger point on channel four shifts in time to maintain triggering at the same point on the reflected signal (the combined signal acting as a trigger signal).

In fact, the reference signals are not changing in phase, but for the above reason, the phase change does show up on the oscilloscope. Tests were conducted to ensure that the phase change of the two frequencies were independent. The phase change data was therefore extracted from channels two and three, the reference signals, rather than the combined, reflected signal.

4.3.1 Data Acquisition

The GP-IB card in the computer is used both for acquiring the requisite data and for controlling the oscilloscope. The card allows the use of various high level computer languages for data acquisition. By installing a device driver program in the C-drive of the computer, programs can operate with the interface card and send commands and receive data from the oscilloscope.

The oscilloscope itself is programmed with a large number of specific commands. These commands can be combined in various ways to gather specific data from the waveforms displayed by the oscilloscope or to control the way waveforms are displayed.

The oscilloscope presents the microwave data as voltage-time sine waves on its screen. These digitally generated waveforms are updated with each trigger pulse. Each update results in a phase change of the two reference signals during a motor test firing.

Phase data from the test signals is acquired by recording the position of a single point on each sine wave. The oscilloscope is initially set at a horizontal resolution of 50 picoseconds/division (screen width 10 divisions). Measurements are made of the peak-to-peak voltage for each frequency. By using the commands inherent to the oscilloscope, the voltage of each waveform is sequentially measured at a point two screen divisions from the left edge of the screen (the trigger point, t=16.0 nsec). Figure 35 shows two successive measurements of the voltage at a fixed time point for the test channels. The phase change is found from the voltage data using the following formulas.

$$\phi_1 = \arcsin(2v_1/A) \qquad\qquad [4.1]$$

$$\phi_2 = \arcsin(2v_2/A) \qquad\qquad [4.2]$$

$$\Delta\phi = \phi_2 - \phi_1 \qquad\qquad [4.3]$$
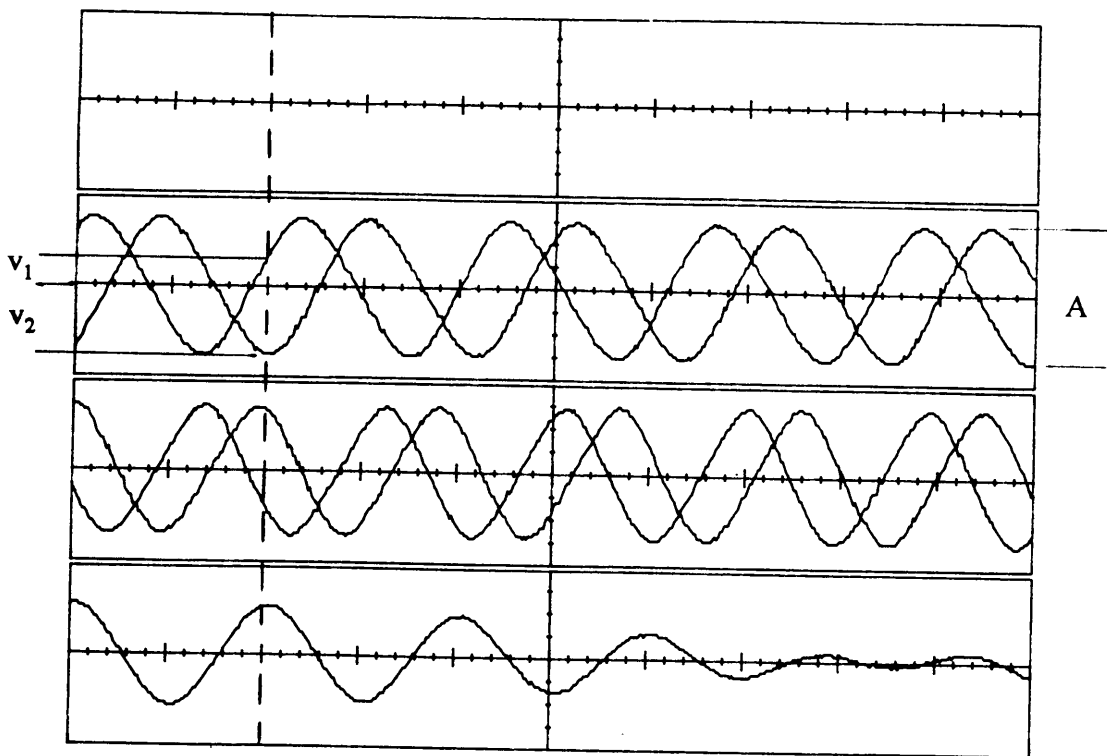
Figure 35. Voltage measurement for phase change determination.

where ϕ_1 is the phase of the signal at time t_1.
                         ϕ_2 is the phase of the signal at time t_2.
                         A   is the peak-to-peak voltage of the signal.

Since the data is acquired at a known constant rate, the time rate of phase change of the microwave signals is found by dividing equation 4.3 by the time interval between points.The BASIC commands used to acquire and store this data for one channel are listed in table 6.

This command string is sent to channels two and three in a continuous loop at a data acquisition rate which is high enough to make the data reduction programs valid.

A minimum value of the data acquisition rate was found to be around 100 Hz for a burn rate of one cm/sec. This was found from the simulations to still allow the data reduction techniques to work, though with much more limited burn rate resolution. Unfortunately, the oscilloscope, as currently configured was unable to make these measurements at more than two measurements per second. Nonetheless, the experimental testing and results are valuable in showing how the system works and its ability to use two frequencies simultaneously with each acting independently. The following section presents the data manipulation process to be followed with experimentally derived data.

4.3.2 Data Manipulation

Data manipulation encompasses three major steps. First, the raw data acquired is converted into time-rate of phase change data for both frequencies. This process was shown in figure 35. The formulas developed in section 2 are then used to extract the actual phase change of the vector reflected from the propellant surface. This data can

Table 6. Commands for making phase measurements.

10 TIMEBASE:RANGE 500 ps	;SET TIMEBASE TO 50ps/div
20 MEAS:SOUR:CHAN2:VPP?	;MEASURE THE PEAK-TO- ;PEAK VOLTAGE OF CHAN2
30 MEAS:SOUR:CHAN3:VPP?	;REPEAT FOR CHANNEL 3
40 MEAS:SOUR:CHAN2	;SET MEASUREMENT TO ;CHAN2
50 MEAS:VTIME? 16.1 ns	;MEASURE THE VOLTAGE OF ;CHAN2 AT 16.1 ns
60 MEAS:SOUR:CHAN3	;SET MEASUREMENT TO ;CHAN3
70 MEAS:VTIME? 16.1 ns	;MEASURE THE VOLTAGE OF ;CHAN3 AT 16.1 ns
80 GO TO 40	;REPEAT VTIME ;MEASUREMENTS

then be used with formula [1.0] to calculate and display burn rate curves for both frequencies. Mismatches in the two curves can be corrected by fine-tuning the values for microwave wavelength in the propellant.

These data manipulation tasks are in general very simple and are easily carried out by the computer using a high level program with appropriate inputs by the operator.

5. TESTING AND TEST RESULTS

5.1 Test Objectives

The primary objective of the test program was to provide a controlled environment under which the major assumptions developed in earlier sections were proved or disproved. This required an independent method of measuring the parameters being measured by the microwave system.

The primary assumption involving the measurement system was the independence of each of the two signals (frequencies 1 and 2) during operation. Verification of this assumption was achieved by making phase change measurements operating one frequency at a time and comparing the results to operation with both frequencies simultaneously. This testing was independent of the testing used to confirm assumptions in the two frequency model.

The assumptions from the two frequency model included the relationships between total vector phase change and the phase change of the vector reflected from the propellant surface. The computer simulations have shown the technique used to extract this information functions adequately using two frequencies.

Due to the equipment limitations encountered and explained in section 4, test results which could be compared with the simulation results given in section 3 cannot be be presented at this time. Within these limitations, tests were conducted which were similar to earlier laboratory testing of the single frequency system.

5.2 Test Procedures

Two types of test were done on the system The first type was static measurement of the phase change of the reflected signals using both frequencies simultaneously and then separately. In this test, phase data was recorded manually off the oscilloscope

74

screen. A comparison of the phase change was then made. The second type of test dynamically measured the regression rate of a moving reflector and used the computer and data acquisition program to obtain the data. This measurement was also done in a single frequency and dual frequency mode. Both test methods used a reflector mounted on a moving platform which simulated the regression of the propellant surface. This device was used by Holly [1] in his laboratory testing of the single frequency system. A schematic of the device is shown in figure 36. A ten inch diameter steel plate was used to reflect the microwave signals from the horn. The plate is attached to a sliding platform which in turn is connected to a gear train driven by a variable speed DC motor.

5.3   Test Results

5.3.1   Static Position Measurement

This test was conducted by setting the reflector 3.0 cm from the microwave horn. The reflector was moved in half centimeter increments until it reached the horn. At each point the zero voltage time change of each signal was determined from the previous measurement. Phase change calculation was performed by dividing the time change by the waveform period in picoseconds, then multiplying by 2π. The reflector movement, Δx, is obtained through the use of the burn rate formula modified for static conditions.

Table 7 contains the test results for simultaneous use of both frequencies, and table 8 contains the results of operating one frequency at a time. The largest errors occur at the end of the measurement (position of 0.0 cm) which is probably due to the interaction of the reflector with the electric field around the horn. This would not occur in an actual test due to the motor casing being in the way. Otherwise, the errors are small, with the maximum occurring at 0.5 cm for both measurements. A major limitation of accuracy in these measurements is the screen resolution.
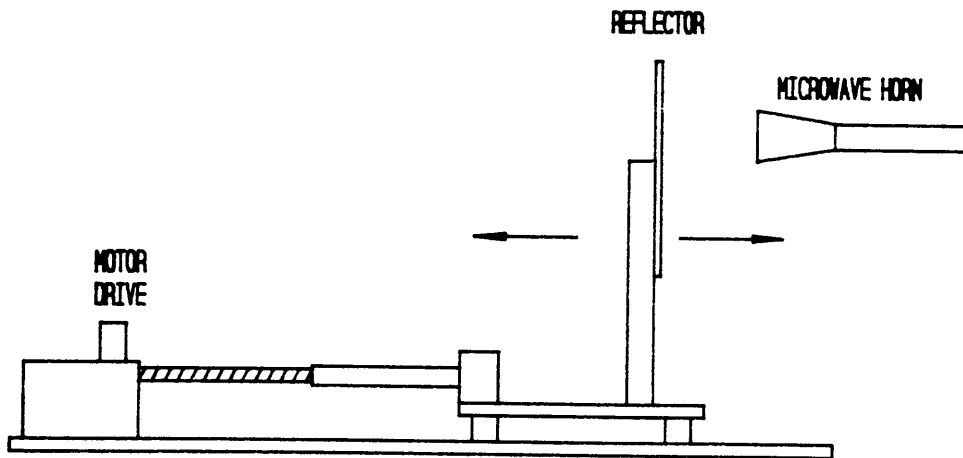
Figure 36. Moving reflector test fixture.

Table 7. Static Test Results, Dual-Frequency Operation.

Position(cm)	$\Delta\phi$(rad)	Δx (cm)	x (cm)
F1(9.12 Ghz):			
3.0			3.0
	2.005	0.525	
2.5			2.475
	2.005	0.525	
2.0			1.950
	1.375	0.360	
1.5			1.590
	1.718	0.450	
1.0			1.140
	2.005	0.525	
0.5			0.615
	1.375	0.360	
0.0			0.255
F2(10.31 Ghz):			
3.0			3.0
	2.008	0.465	
2.5			2.535
	2.526	0.585	
2.0			1.950
	1.555	0.360	
1.5			1.590
	1.814	0.420	
1.0			1.170
	2.397	0.555	
0.5			0.615
	1.555	0.360	
0.0			0.255

Table 8. Static Test Results, Single Frequency Operation.

Position(cm)	$\Delta\phi$(rad)	Δx (cm)	x (cm)
F1(9.12 Ghz):			
3.0			3.0
	2.06205	0.540	
2.5			2.460
	1.833	0.480	
2.0			1.980
	1.375	0.360	
1.5			1.620
	1.776	0.465	
1.0			1.155
	1.890	0.495	
0.5			0.660
	1.375	0.360	
0.0			0.300
F2(10.31 Ghz):			
3.0			3.0
	2.591	0.600	
2.5			2.400
	2.267	0.525	
2.0			1.875
	1.814	0.420	
1.5			1.455
	2.037	0.480	
1.0			0.975
	2.202	0.510	
0.5			0.465
	1.684	0.390	
0.0			0.075

In these and other measurements the resolution of the waveforms resulted in possible errors of plus or minus ten percent for phase measurements.

Figure 37 contains the position data for both measurements in graphic form. For the single frequency measurements the frequencies diverge to a greater extent than that occurring during dual frequency operation. Coupling between the frequencies could be occurring. However, the inherent errors in measurement and the divergence from the actual measurement could account for the result.

5.3.2 Dynamic Testing

The dynamic measurements are similar to the static position measurements. In these tests, however, the computer and data acquisition program was used to measure the regression rate of the reflector device.

The regression rate was set to 0.44 cm/sec and 3.0 cm total travel. This rate was fixed by the maximum data rate available (2.95 Hz) and the lower speed limit of the reflector motor drive. The regression rate curves are shown in figure 38. This figure shows the data for each frequency during dual frequency operation and with one frequency operating at a time. Large errors occur in both cases due mainly to the resolution error involving the oscilloscope since this test eliminates multiple reflections by using a single reflector moving at a constant rate. In the case of voltage measurements, these errors can be greater than 70%, depending upon the voltage level. In the tests performed such large errors did occur which makes it difficult to determine the accuracy of these results. More accurate measurement of the phase change is clearly required.

SINGLE FREQUENCY OPERATION
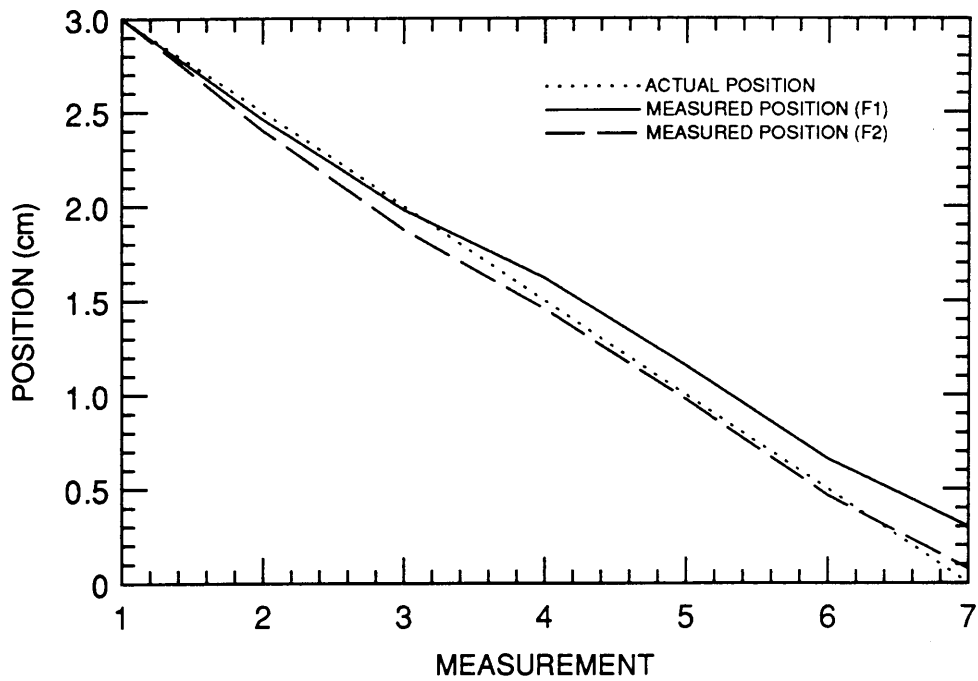
DUAL-FREQUENCY OPERATION
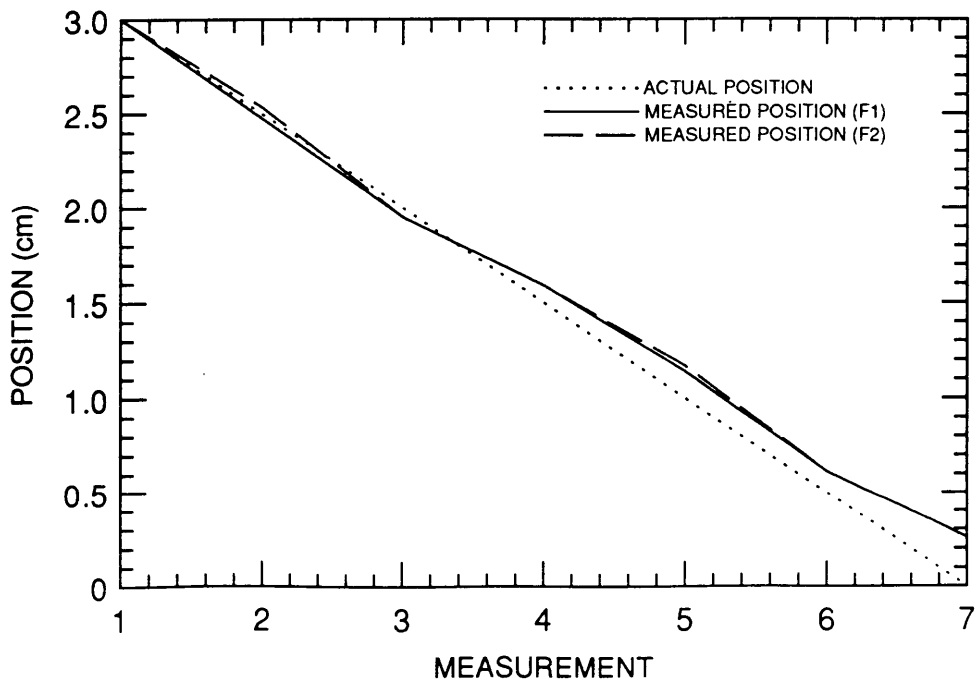
Figure 37. Single and dual frequency position measurements.
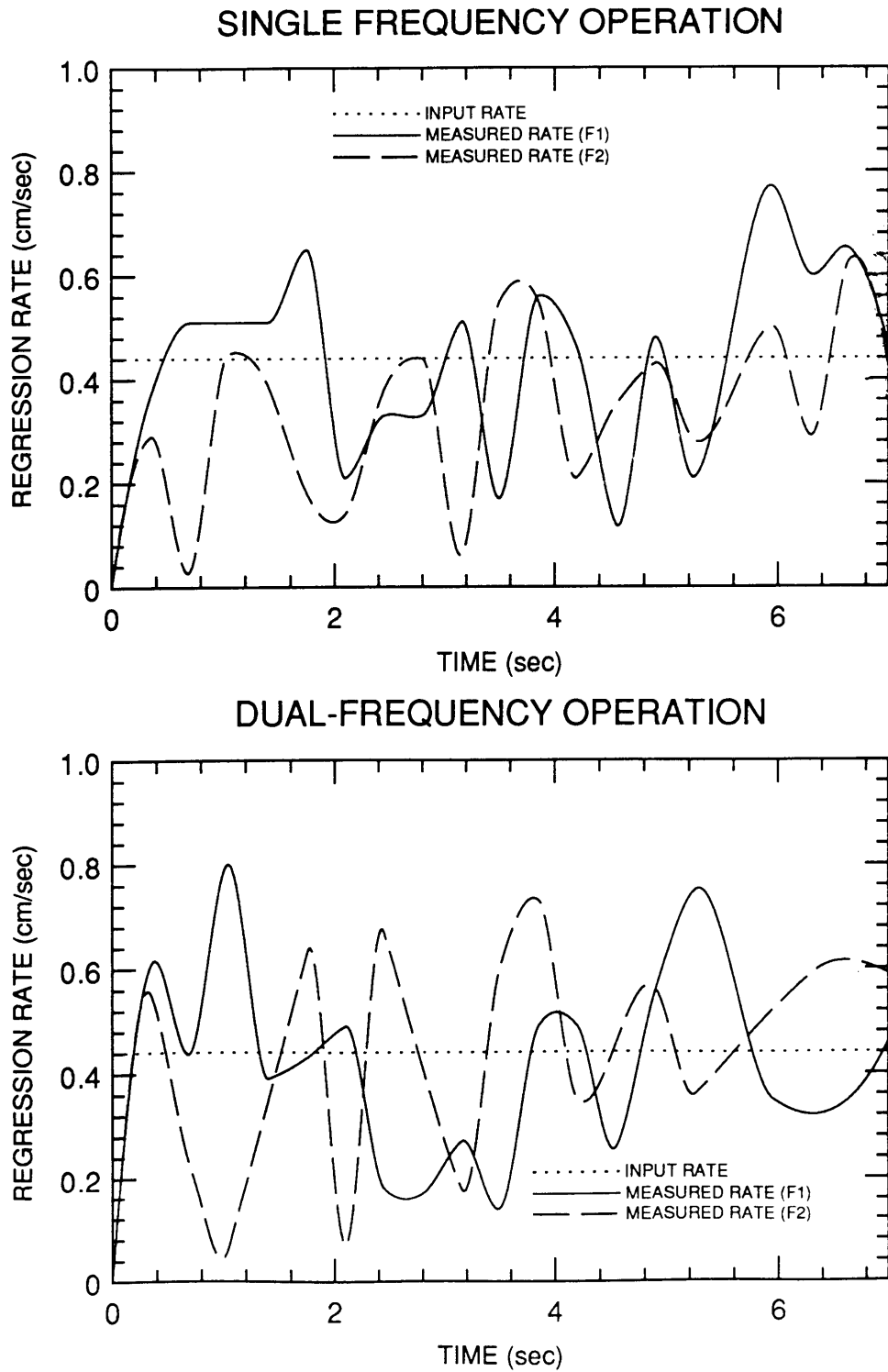
Figure 38. Regression rate measurements in single and dual frequency mode.

An example of the advantage of dual-frequency measurements, figure 39 contains a single regression rate curve for the average of the simultaneous dual frequency measurements. Comparing with figure 38, the maximum error has been reduced from over 100% to less than 55%. Though the error remains large, in this case it is still much smaller than that obtainable with a single frequency.
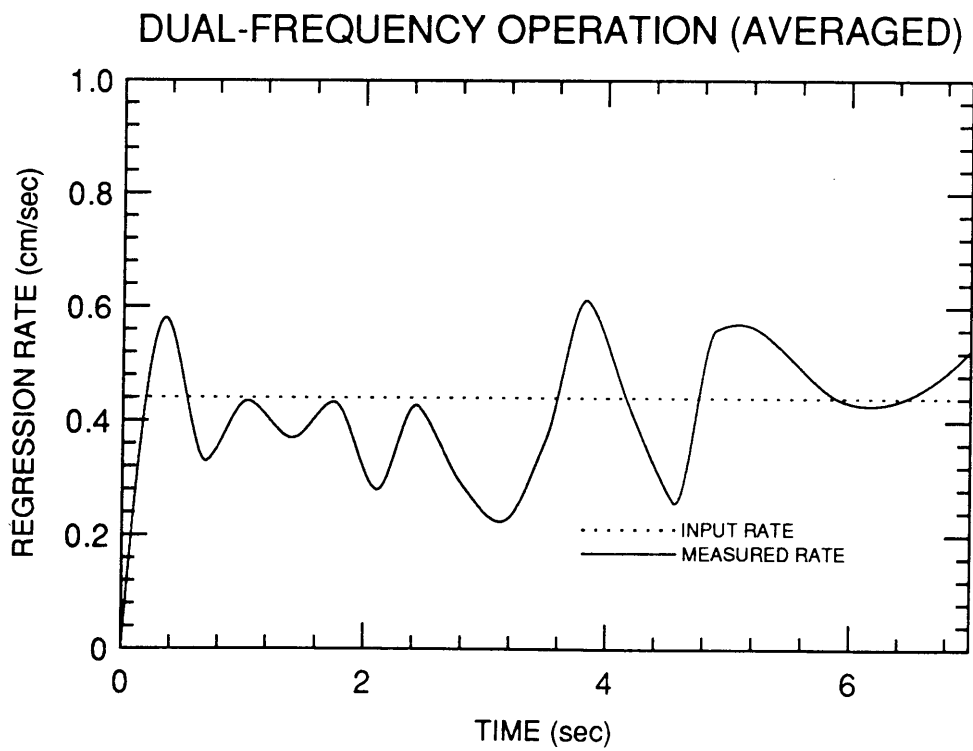
Figure 39. Measured regression rate using dual-frequency averaging.

6.   CONCLUSIONS AND RECOMMENDATIONS

The dual frequency measurement system described in this thesis shows promise in its ability to reduce measurement errors due to various factors. This is an improvement over the single frequency system, though the improvement has not reached the point at which it could replace all other measurement systems.

However, in all cases investigated, a significant reduction in error could be observed. This compares with no error reduction when using a single frequency. In cases where secondary reflections are offset by about 180 degrees, the error reduction is substantial. In other cases it provides limited suppression of secondary reflection errors.

The system was not able to conclusively prove its ability to eliminate knowledge of the microwave wavelength. Although the system of equations given in chapter 2 (equations 2.3,2.4 and 2.5) seems to be a closed system allowing iteration of the value of wavelength until all equations are satisfied, the simulations were not able to show this due to the limitations of the simulation program. Simulation 1 did show the ability of the integration technique to eliminate knowledge of the wavelength with the restrictions of no extraneous reflections and a constant burn rate. These are, in most cases, unrealistic restrictions. Also, This technique does not need the two frequencies, making its use here somewhat superfluous.

Several of the simulations showed the effect a larger frequency separation had on cases where the physical parameters are unchanged. In general the larger frequency separation resulted in a larger error reduction. The size of the frequency separation is limited by the hardware used (waveguides and sources) but for a certain motor geometry there could be an optimum frequency separation which would not necessarily be the largest possible. Although the simulations point to this as the reason for the error reduction, there is some doubt as to it being strictly the result of motor geometry and

frequency separation and not an effect of imperfections in the model or the simulation program.

The simulations give an idea of the system's ability to deal with certain situations which will vary depending upon the motor geometry and microwave frequencies used. Due to the equipment limitations encountered, these abilities could not be fully confirmed. Developing and operating the system has however proved its ability to use two frequencies simultaneously. The two types of dual frequency tests conducted, position measurement and dynamic rate measurement, were compared with tests done using one frequency at a time. There was no significant deviation between the two for each type of test. This is qualified by the fact that large inherent measurement errors could be present, especially in the dynamic measurements, which could skew the results. This testing was invaluable in showing how the system works and that it could work. It also provided insight into the direction further research should take.

Continuing research should focus in parallel on the areas of hardware improvements and enhanced data reduction to enable high data rate sampling. The crude data reduction method used in the simulations did not take full advantage of the dual frequency system. Since the phase data returned by the system is a combination of phase changes at different frequencies (and was modeled as such), the use of Fast Fourier Transform (FFT) methods could improve data reduction. By looking at the FFT of both signals, it could be possible to filter out the unwanted frequencies representing the signals from extraneous reflections. A major impediment to use of FFT techniques is the magnitude variation of each reflection signal which is incompatible with use of the FFT method.

The 20 Ghz oscilloscope used in these experiments has proven indispensable for characterizing the behavior of the dual frequency system. The ability to look at the actual microwave signals, both mixed and separately, enabled development of the system as

presently configured and has improved the understanding of the measurement methods. The oscilloscope is not optimized for the data acquisition required for this type of phase change measurement. Earlier testing used a phase-gain meter which required a reference and test signal input for the single frequency system. Two phase-gain meters would provide phase and magnitude data of greatly improved quality over the present data. This would also eliminate the measurement error problem encountered with the oscilloscope (see chapter 5). Use of the phase-gain meters would require filtering of the test signal (currently sampled as a single signal) to extract the individual signals for each frequency used. This has already been done by using a waveguide T-section and adjustable waveguide shorts as filters on each branch, so does not present much of a problem. Improved microwave sources, such as the solid state, microprocessor-controlled units now available would greatly increase the capability of the system. Such units provide adjustable power levels, high frequency tuning accuracy and dual frequency capability. These sources would also improve the resolution of the oscilloscope, since they would provide a more coherent signal for triggering and display.

These recommendations could provide the basis for a continuing research program to improve and eventually test the dual frequency system during a live rocket motor firing. Such further work is needed to demonstrate the advantages of this method, which can be used with little extra effort than that required for the single frequency system.

BIBLIOGRAPHY

1.   Holly, H.M., "An Analysis of Solid Propellant Burn Rate Information Obtained from a Microwave Doppler Phase Shift Interferometer", M.S. Thesis, Virginia Polytechnic Institute and State University, Department of Mechanical Engineering, Blacksburg, VA, November 1981.

2.   Wood, H.L., O'Brien, W.F., and Dale, C.B., "Measurement of Solid Propellant Burning Rates Employing Microwave Techniques," Proceedings of the 6th International Symposium on Air Breathing Engines, Paris, France, June 1983.

3.   Kliger, J.J., "Measurement of Solid Propellant Burning Rates in a Slab-Motor Environment Using a Microwave Technique," M.S. Thesis, Virginia Polytechnic Institute and State University, Department of Mechanical Engineering, Blacksburg, VA, January 1984.

4.   Boley, J.B., "Microwave Data Reduction Technique for Calculation of Solid Propellant Burning Rates," M.S. Thesis, Virginia Polytechnic Institute and State University, Department of Mechanical Engineering, Blacksburg, VA, November 1984.

5.   Waesche, R.H.W., and O'Brien, W.F., "Evaluation of Techniques for Direct Measurement of Burning Rates in Nozzleless Motors," ARC Report, Atlantic Research Corporation, Gainesville, VA, September 1987.

APPENDICES

A.   Simulation Program MWSIM.FOR

B.   Data Acquisition Program HPV.BAS

A. Program MWSIM.FOR

```
C    VARIABLE DEFINITIONS:
C
C       X= X COMPONENT OF TOTAL VECTOR
C       Y= Y COMPONENT OF TOTAL VECTOR
C       XB=X COMPONENT OF BURNING SURFACE VECTOR
C       YB=Y COMPONENT OF BURNING SURFACE VECTOR
C       XR=X COMPONENT OF SECONDARY VECTOR
C       YR=Y COMPONENT OF SECONDARY VECTOR
C       XC=X COMPONENT OF DIFFERENCE VECTOR
C       YC=Y COMPONENT OF DIFFERENCE VECTOR
C       PH= PHASE OF DIFFERENCE VECTOR
C       DPH= PHASE CHANGE OF DIFFERENCE VECTOR
C       R= BURN RATE
C       T= TIME
C       LAMBDA= MICROWAVE WAVELENGTH
C       PRATIO= POWER RATIO OF FREQUENCY 1 OVER 2
C       F1, F2= FREQUENCIES
C       FRATIO= FREQUENCY RATIO
C       VA= MAGNITUDE OF FIXED VECTOR
C       VB= MAGNITUDE OF BURNING SURFACE VECTOR
C       VR= MAGNITUDE OF SECONDARY VECTOR
C       VBE= FINAL MAGNITUDE OF BURNING SURFACE VECTOR
C       VRE= FINAL MAGNITUDE OF SECONDARY VECTORC
C       ANGA= INITIAL ANGLE OF FIXED VECTOR
C       ANGB= INITIAL ANGLE OF VB
C       ANGR= INITIAL ANGLE OF VR
C       W= PROPELLANT WEB THICKNESS
C       RRB= ROTATION RATE OF VB
C       RRR= ROTATION RATE OF VR
C       FRB= FINAL ROTATION RATE OF VB
C       FRR= FINAL ROTATION RATE OF VR
C       TB= BURN TIME
C       DT= DELTA TIME
C
C    FILE NAMES
C
C       BR1.DAT= BURN RATE DATA FOR FREQ 1
C       BR2.DAT= BURN RATE DATA FOR FREQ 2
C       VC1.DAT= X,Y COMPONENTS OF TOTAL VECTOR, FREQ 1
C       VC2.DAT= X,Y COMPONENTS OF TOTAL VECTOR, FREQ 2
C       DVC1.DAT=X,Y COMPONENTS OF DIFFERENCE VECTOR, F1
C       DVC2.DAT=X,Y COMPONENTS OF DIFFERENCE VECTOR, F2
C
C234567
        DIMENSION XB(1000),YB(1000),XR(1000),YR(1000),
       +X(1000),Y(1000),DVC(1000),XC(1000),YC(1000),PH(1000),
       +DPH(1000),R(1000),VC(1000),T(1000)
```

```
      REAL LAMBDA
   10 OPEN(4,FILE='A:DVC1.DAT')
   20 OPEN(2,FILE='A:VC1.DAT')
   60 PI=3.14159
C
C   GET INITIAL VALUES FOR FREQUENCY 1 AND FREQ RELATIONSHIP
C
      WRITE(*,*)' ENTER MICROWAVE POWER RATIO FOR
     +FREQUENCIES 1 OVER 2'
      READ(*,*)PRATIO
      WRITE(*,*)' ENTER FREQUENCIES FOR CHANNEL 1 AND 2
     +IN GHz'
      READ(*,*)F1,F2
      FRATIO=F2/F1
   70 WRITE(*,*)' ENTER MAGNITUDES OF FIXED(Va),
     +BURNING(Vb), AND '
      WRITE(*,*)'SECONDARY (Vr) VECTORS IN mV FOR CHANNEL 1'
   90 READ(*,*)VA, VB, VR
C
C   CALCULATE INITIAL MAG OF VECTORS FOR FREQ 2
C
      VB2=VB/PRATIO
      VR2=VR/PRATIO
      WRITE(*,*)' ENTER INITIAL ANGLE OF Va, Vb AND Vr IN
      DEGREES'
      READ(*,*) ANGA,ANGB, ANGR
C
C   CONVERT ANGLES TO RADIANS
C
      ANGB=ANGB*PI/180.
      ANGR=ANGR*PI/180.
      ANGA=ANGA*PI/180.
      WRITE(*,*)' ENTER PROPELLANT WEB THICKNESS AND MWAVE'
      WRITE(*,*)'WAVELENGTH (FOR FREQ 1) IN cm '
      READ(*,*)W,LAMBDA
C
C   ENTER VECTOR DATA AND CONVERT VALUES FOR FREQ 2
C
      WRITE(*,*)' ENTER ROTATION RATES OF Vb AND Vr IN
     +rad/sec'
      READ(*,*)RRB, RRR
      RRB2=RRB*FRATIO
      RRR2=RRR*FRATIO
      WRITE(*,*)' ENTER FINAL ROTATION RATES OF Vb AND Vr'
      READ(*,*)FRB,FRR
      FRB2=FRB*FRATIO
      FRR2=FRR*FRATIO
      WRITE(*,*)' ENTER FINAL MAGNITUDES OF Vb AND Vr IN mV'
      READ(*,*)VBE,VRE
      VBE2=VBE/PRATIO
      VRE2=VRE/PRATIO
```

```
      WRITE(*,*)' ENTER VALUE FOR DELTA T AND TOTAL BURN
     +TIME IN sec'
      WRITE(*,*)' (LIMIT TOTAL ITERATIONS TO UNDER 1000)'
      READ(*,*)DT,TB
C
C    CALCULATE NUMBER OF ITERATIONS FOR GIVEN DELTA T
C
      K = TB/DT+1
C
C    BEGIN CALCULATION OF X AND Y COMPONENTS FOR
C    TOTAL VECTOR
C
  220 XA=VA*COS(ANGA)
      YA=VA*SIN(ANGA)
C
C    SET UP ORIGINAL MAGNITUDE VALUES
C
      VBO=VB
      VRO=VR
      DO 350 N=1,K
      XB(N)=VB*COS(ANGB)
      YB(N)=VB*SIN(ANGB)
      XR(N)=VR*COS(ANGR)
      YR(N)=VR*SIN(ANGR)
C
C    TOTAL VECTOR COMPONENT VALUES
C
      X(N)=XA+XB(N)+XR(N)
      Y(N)=YA+YB(N)+YR(N)
      WRITE(2,*)X(N),Y(N)
C
C    CALCULATE NEW ANGLES AND NEW MAGNITUDES
C
      ANGB=ANGB+DT*(RRB+(FLOAT(N)-.5)*(FRB-RRB)/FLOAT(K))
      ANGR=ANGR+DT*(RRR+(FLOAT(N)-.5)*(FRR-RRR)/FLOAT(K))
      VB=VB+(VBE-VBO)/FLOAT(K)
      VR=VR+(VRE-VRO)/FLOAT(K)
  350 CONTINUE
C
C    CALCULATE DIFFERENCE VECTOR COMPONENTS
C
      DO 400 N=2,K
      XC(N)=X(N)-X(N-1)
      YC(N)=Y(N)-Y(N-1)
      WRITE(4,*)XC(N), YC(N)
  400 CONTINUE
C
C    CALCULATE DIFFERENCE VECTOR PHASE
C
      DO 460 N=2,K
      PH(N)=ATAN2(YC(N),XC(N))
```

```
   460 CONTINUE
       CLOSE(4,STATUS='KEEP')
C
C    CHECK ROUTINE FOR FREQ 2 CALCULATION.
C    IF FREQ 2 DONE GO TO END OF PROGRAM.
C
       IF(FL2.EQ.9.)THEN
       OPEN(8,FILE='A:BR2.DAT')
       GO TO 480
       END IF
       OPEN(8,FILE='A:BR1.DAT')
C
C    CALCULATE PHASE CHANGE OF DIFFERENCE VECTOR
C    CALCULATE AND STORE BURN RATE AND TIME
C
   480 K=K-1
       WRITE(8,*)T(1),R(1)
       DO 520 N=2,K
C
C    ROUTINE FOR PHASE CROSSING 180 TO -180 DEGREES
C
       IF(PH(N+1).GT.0.0.AND.PH(N).LT.0.0)THEN
       DPH(N+1)=DPH(N)
       GOTO 490
       END IF
       IF(PH(N+1).LT.0.0.AND.PH(N).GT.0.0)THEN
       DPH(N+1)=DPH(N)
       GO TO 490
       END IF
       DPH(N+1)=(PH(N+1)-PH(N))/DT
C
C    BURN RATE CALCULATION
C
   490 R(N+1)=DPH(N+1)*LAMBDA/(4.*PI)
       T(N+1)=DT*(N+1)
       WRITE(8,*)T(N+1),R(N+1)
   520 CONTINUE
C
C    FOLLOWING LINES USED FOR CONVERSION OF SOME INPUTS
C    TO FREQ 2 PARAMETERS
C
       IF(FL2.EQ.9.)GO TO 530
       FL2=9.
       K=K+1
       VA=VA/PRATIO
       LAMBDA=LAMBDA/FRATIO
       VB=VB2
       VR=VR2
       VBE=VBE2
       VRE=VRE2
```

```
      RRB=RRB2
      RRR=RRR2
      FRB=FRB2
      FRR=FRR2
      CLOSE(2,STATUS='KEEP')
      CLOSE(8,STATUS='KEEP')
      OPEN(2,FILE='A:VC2.DAT')
      OPEN(4,FILE='A:DVC2.DAT')
C
C    INPUT INITIAL ANGLES FOR FREQ 2
C
      WRITE(*,*)' ENTER INITIAL ANGLES FOR VECTORS OF
     +CHANNEL 2'
      WRITE(*,*)'  (Va,Vb AND Vr)'
      READ(*,*)ANGA,ANGB,ANGR
      ANGB=ANGB*PI/180.
      ANGR=ANGR*PI/180.
      ANGA=ANGA*PI/180.
      GO TO 220
  530 STOP
      END
```

B.   Program HPV.BAS

```
REM SET FILENAMES OF OUTPUT FILES

10 INPUT "input data file name ";GNAME$
20 HNAME$=GNAME$+"1"

REM OPEN THE PORTS FOR THE GPIB BUS

30 OPEN "PC488A" FOR OUTPUT AS #1
40 OPEN "PC488A" FOR INPUT AS #2
50 OPEN HNAME$ FOR OUTPUT AS #3

REM CLEAR THE SCOPE AND SETUP FOR DATA ACQUISITION

60 PRINT #1, "ABORT"
70 PRINT #1, "CLEAR"
80 PRINT #1, "TERM 13 10"
90 PRINT #1,"OUTPUT 22;*RST"
100 PRINT #1,"OUTPUT 22;:AUTOSCALE"
110 PRINT #1,"OUTPUT 22;:TIMEBASE:RANGE 500ps"
120 PRINT #1,"OUTPUT 22;:ACQUIRE:TYPE AVERAGE "
130 PRINT #1,"OUTPUT 22;:DISPLAY:VMARKER ON"

REM MEASURE AND INPUT THE PEAK-TO-PEAK VOLTAGES
REM FOR CHANNELS 2 AND 3

140 PRINT #1,"OUTPUT 22;:MEAS:SOURCE CHAN2;VPP?"
150 PRINT #1,"ENTER 22"
160 PRINT #3,INPUT$(12,#2);CHR$(13):
170 ON ERROR GOTO 200
180 IF EOF(2) THEN 200
190 PRINT ASC(INPUT$(1,#2));
200 PRINT #1,"OUTPUT 22;:MEAS:SOURCE CHAN3;VPP?"
210 PRINT #1,"ENTER 22"
220 PRINT #3,INPUT$(12,#2);CHR$(13):
230 ON ERROR GOTO 260
240 IF EOF(2) THEN 260
250 PRINT ASC(INPUT$(1,#2));
260 CLOSE #3

REM SET UP SCOPE AND FILES FOR VOLTAGE DATA

270 PRINT #1,"OUTPUT 22;:ACQUIRE:TYPE AVERAGE"
280 HNAME$=GNAME$+"3"
290 OPEN HNAME$ FOR OUTPUT AS #3
300 PRINT #1,"OUTPUT 22;:DISPLAY:TMARKER ON"
310 PRINT #1,"OUTPUT 22;:MEAS:PRECISION FINE"
```

```
REM QUERY USER FOR TYPE OF DATA ACQUISITION
REM AND NUMBER OF POINTS

320 INPUT"ENTER NUMBER OF DATA POINTS TO BE ACQUIRED";J
330 INPUT"ENTER 1, 2, 3 FOR ACQUISITION OF FREQ 1, 2, OR
    BOTH";K
340 INPUT"PRESS ENTER TO BEGIN ACQUISITION";G$+
350 FOR N=1 TO J
360 IF K=2 THEN GOTO 440

REM    ACQUIRE VOLTAGE OF CHAN 2 AT 16.1 ns

370 PRINT #1,"OUTPUT 22;:MEAS:SOUR CHAN2;VTIME? 16.1 ns"
380 PRINT #1,"ENTER 22"
390 PRINT #3,INPUT$(12,#2);CHR$(13):
400 ON ERROR GOTO 440
410 IF EOF(2) THEN 440
420 PRINT ASC(INPUT$(1,#2));
430 IF K=1 THEN GOTO 500

REM    ACQUIRE VOLTAGE OF CHAN 3 AT 16.1 ns

440 PRINT #1,"OUTPUT 22;:MEAS:SOUR CHAN3;VTIME? 16.1 ns"
450 PRINT #1,"ENTER 22"
460 PRINT #3,INPUT$(12,#2);CHR$(13):
470 ON ERROR GOTO 500
480 IF EOF(2) THEN 500
490 PRINT ASC(INPUT$(1,#2));
500 NEXT N

REM END DATA ACQUISITION

510 INPUT "PAUSE 385";C
520 CLEAR:CLOSE
530 END
```

The vita has been removed from the scanned document